Computers and Concrete, *Vol. 22, No. 6 (2018) 573-592*
DOI: https://doi.org/10.12989/cac.2018.22.6.573

Flexural/shear strength of RC beams with longitudinal FRP bars An analytical approach

Parthena-Maria K. Kosmidou[a], Constantin E. Chalioris[*] and Chris G. Karayannis[b]

Department of Civil Engineering, Scholl of Engineering, Democritus University of Thrace, Laboratory of Reinforced Concrete and Seismic Design of Structures, Xanthi 67100, Greece

(Received June 19, 2018, Revised September 18, 2018, Accepted December 18, 2018)

Abstract. An analytical methodology for the calculation of the flexural and the shear capacity of concrete members with Fibre-Reinforced-Polymer (FRP) bars as tensional reinforcement is proposed. The flexural analysis is initially based on the design provisions of ACI 440.1R-15 which have properly been modified to develop general charts that simplify computations and provide hand calculations. The specially developed charts include non-dimensional variables and can easily be applied in sections with various geometrical properties, concrete grade and FRP properties. The proposed shear model combines three theoretical considerations to facilitate calculations. A unified flexural/shear approach is developed in flow chart which can be used to estimate the ultimate strength and the expected failure mode of a concrete beam reinforced with longitudinal FRP bars, with or without transverse reinforcement. The proposed methodology is verified using existing experimental data of 138 beams from the literature, and it predicts the load-bearing capacity and the failure mode with satisfactory accuracy.

Keywords: reinforced concrete (RC); fibre-reinforced polymer (FRP) bars; flexure; shear; analytical model

1. Introduction

Corrosion of steel reinforcing bars embedded in concrete beams and girders has been the cause of severe structural damages and of high costs in repair and maintenance. Several researchers investigated the harmful effects of corrosion on Reinforced Concrete (RC) structural members and especially on their durability properties (Zeris *et al.* 2014, Bousias *et al.* 2004). Because of that, there has been recent interest in the potential use of new reinforcing composite materials that can prevent or minimize corrosion-related issues and can be used efficiently for repair or/and strengthening of RC structures (Tan 2002, Vougioukas *et al.* 2005, Bouguerra *et al.* 2011, Kang and Ary 2012, Fang *et al.* 2016, Tsonos 2009, Ha *et al.* 2013, Liang *et al.* 2017a). The application of Fibre-Reinforced-Polymer (FRP) bars is a promising alternative to conventional steel longitudinal reinforcing bars in concrete members. FRP stirrups have also been used as transverse reinforcement in shear critical concrete beams and special shear models have been developed (El-Sayed and Soudki 2011, Oller *et al.* 2015, Said *et al.* 2016, Johnson and Sheikh 2016).

FRPs exhibit high tensile strength, excellent corrosion resistance, non-magnetization properties, light weight and reliable durability. However, the most commonly used FRP materials demonstrate some shortcomings with regards to steel reinforcement. They have relatively lower modulus of elasticity, high cost and non-yielding characteristics (Konsta-Gdoutos and Karayannis 1998, Chalioris *et al.* 2016, Liang *et al.* 2016, Ghatefar *et al.* 2017). Nevertheless, a newly developed glass FRP bar has recently been addressed and experimentally investigated by Ju *et al.* (2017). This advanced glass FRP bar was fabricated by thermosetting a braided pultrusion process to form the outer fibre ribs and proved to overcome the lower modulus of elasticity and bond strength compared to a steel bar.

Further, wider and deeper cracks coupled with the relatively low strength and stiffness of FRP materials in the transverse direction result in a questionable contribution of the tensional longitudinal FRP bars as dowel action to the shear capacity of concrete beams compared to the contribution of steel bars. Tureyen and Frosch (2002), El-Sayed *et al.* (2006) observed that the shear strength of FRP reinforced beams without transverse reinforcement is proportional to the axial stiffness of the longitudinal FRP bars and depends on their material properties, but their contribution as dowel action to the shear capacity of the tested beams is lower than that of steel bars. However, recent tests in concrete slabs with carbon and glass FRP bars revealed that the composite bars delayed the load level at which cover spalling occurred in the FRP - concrete which resulted in a greater-than-expected contribution of dowel action with FRP reinforcement (Abdul-Salam *et al.* 2016). Nevertheless, the overall shear capacity of concrete beams with FRP bars and stirrups is considered to be lower than that of conventionally steel RC beams since the shear resisting components of the members with FRPs found to be lower in comparison to the members with steel reinforcement (Oller *et al.* 2015, Marí *et al.* 2014).

Several experimental studies have been reported in the literature to investigate the flexural behaviour of concrete

*Corresponding author, Associate Professor
E-mail: chaliori@civil.duth.gr
[a]Ph.D. Student
[b]Professor

ISSN: 1598-8198 (Print), 1598-818X (Online)

beams reinforced with FPR bars (Masmoudi *et al.* 1998, Toutanji and Saafi 2000, Rafi *et al.* 2008, Shin *et al.* 2009, Barris *et al.* 2009, Lee and Kim 2012, Refai *et al.* 2015, Zhang *et al.* 2015, Ovitigala *et al.* 2016, Goldston *et al* 2016, 2017, Liang *et al.* 2017b, Elgabbas *et al.* 2017). Provisions for the design and construction of concrete structures reinforced with FRP bars are also available (ACI 440.1R-15 2015, CSA S806-12 2002, Fib bulletin 40 2007, CNR-DT 203 2007). The estimation of the ultimate flexural strength of RC beams with tensional FRP bars is usually based on the strain compatibility, the internal force equilibrium and the governed failure mode. Ashour (2006) developed a simplified analytical method to calculate the flexural capacity of concrete beams reinforced with FRP tensional and compressional longitudinal bars. Further, based on test results, Saikia *et al.* (2007) proposed an analytical model for the evaluation of the ultimate strength of concrete beams reinforced with glass FRP bars by a cross-sectional analysis that takes into account the critical slip between the composite bar and the concrete. Torres *et al.* (2012) developed a methodology to determine the flexural capacity of sections with FRP bars by utilizing the general parabolic-rectangular diagram for concrete in compression according to the Eurocode 2 (2004) and by using non-dimensional equations that have been derived independently of the characteristics of concrete and FRP reinforcement.

The analytical work of Zadeh and Nanni (2013) highlighted the lack of ductility occurred in concrete beams reinforced with FRP bars due to the brittle FRP rupture failure mode and specially modified strength reduction factors along with design provisions have been recommended to ensure a reliability level for use in FRP design guidelines for shear and flexure. Recently, an alternative reinforcement technique has experimentally and analytically been investigated in order to improve flexural ductility and at the same time retain the high strength feature of the FRP bars by using the hybrid combination of steel and FRP longitudinal reinforcement (Lau and Pam 2010, Shraideh and Aboutaha 2013, El-Helou and Aboutaha 2015, Bencardino *et al.* 2016, Qin *et al.* 2017, Bui *et al.* 2017). Further, the beneficial re-centering capabilities of super-elastic Shape Memory Alloys (SMA) in RC members have been used to develop a new mechanical-adhesive type coupler for splicing FRP to SMA bars (Alam *et al.* 2010).

The aforementioned literature review reveals that although there are several experimental and analytical contributions on the investigation of the flexural or/and the shear response of concrete members reinforced with FRP bars, the combined investigation of the flexural and the shear strength is rather limited. In this study a numerical approach for the evaluation of the flexural and the shear strength of slender concrete beams reinforced with longitudinal FRP bars and consequently for the prediction of the expected failure mode is proposed. A test program of two concrete beams with various ratios of carbon FRP bars as tensional reinforcement subjected to monotonic loading and failed under flexure and shear is also included herein.

The proposed flexural analysis is based on the design provisions of ACI 440.1R-15 (2015) which have properly been modified in order to develop general charts that facilitate calculations. Further, the calculation of the shear strength is achieved using the theoretical considerations proposed by Oller *et al.* (2015), Marí *et al.* (2014, 2015) which have properly been combined for the purposes of this study. Equations with feasible software implementation are derived and thorough computation flow chart is provided. A typical numerical example for the calculation of the flexural and the shear strength is also included for demonstration. The validity of the analytical approach is checked through extensive comparisons between analytical predictions and test data of 138 concrete beams with various types of FRP bars, which failed under different modes compiled from the present study and 13 existing experimental works of the literature. From these comparisons it is observed that the developed approach predicts with satisfactory accuracy the ultimate load-bearing capacity and the expected failure mode for the majority of the examined cases.

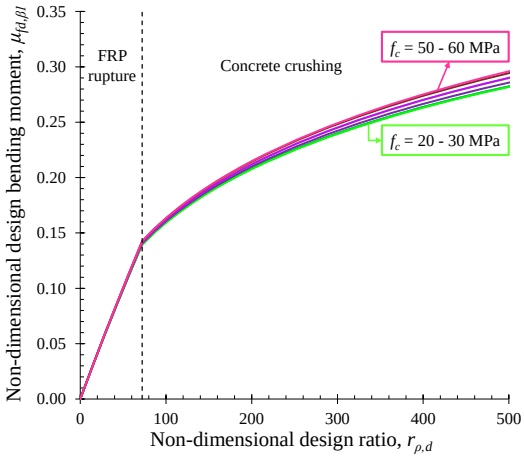

(a) Design chart for ε_{fu}=0.0138 and for various concrete grades

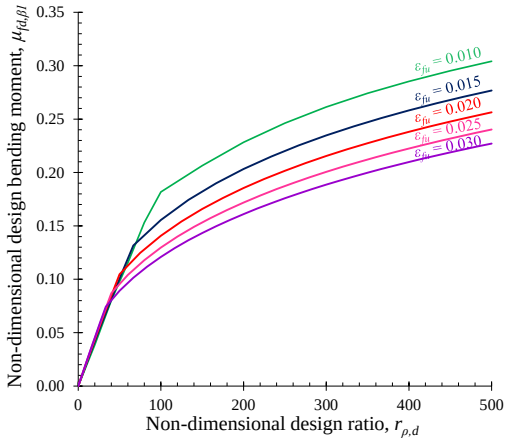

(b) General design chart for various FRP materials

Fig. 1 Design charts for concrete beams reinforced with FRP bars

2. Analytical approach

The aim of the proposed analytical approach is to calculate the ultimate loading bearing capacity of a concrete beam reinforced with longitudinal FRP bars and to predict

the expected failure mode based on the flexural and the shear strength. Thus, two different models are adopted, properly modified and combined.

2.1 Flexural strength

It is known that common design guidelines and provisions provided in Reinforced Concrete Codes for steel reinforcing bars cannot be used directly for concrete members reinforced with FRP bars due to inherent differences in surface deformations, mechanical properties and failure characteristics. In this study, an easy-to-apply procedure has been developed for flexural concrete beams reinforced with FRP bars based on the design guidelines of ACI 440.1R-15 (2015). The aim of the proposed method is to facilitate calculations through the use of specially developed general charts.

These charts are illustrated in Figs. 1 and 2 for the purpose of (i) design and (ii) analysis (without safety factors), respectively, of concrete sections reinforced with FRP bars subjected to bending. The values of the bending moment and the reinforcement ratio in the charts are non-dimensional so that they can be used in sections with various geometrical properties, concrete grade and FRP properties such as ultimate tensile strength, ultimate tensile strain and modulus of elasticity.

In the vertical axes of these charts the values of (i) the non-dimensional design bending moment, $\mu_{fd,\beta 1}$ (Fig. 1) and (ii) the non-dimensional flexural capacity, μ_f (Fig. 2) depend on the geometry of the cross-section and the concrete grade of a beam and can be calculated as follows

$$\mu_{fd,\beta 1} = \frac{M_{Ed}}{bd^2 \beta_1 f_c} \tag{1a}$$

and

$$\mu_f = \frac{M_f}{bd^2 f_c} \tag{1b}$$

where M_{Ed} is the design value of the applied bending moment; and M_f is the flexural capacity without safety factors.

Further, in the horizontal axes of these charts the use of the following special non-dimensional variables is proposed:

(i) In Fig. 1 the non-dimensional design ratio, $r_{\rho,d}$, is defined as the ratio of the FRP reinforcement ratio, ρ_f, to the design balanced ratio, $\rho_{fb,d}$, divided by the design tensile strain of FRP bar, ε_{fu}, and

(ii) in Fig. 2 the non-dimensional ratio, r_ρ, is defined as the ratio of the FRP reinforcement ratio, ρ_f, to the balanced ratio, ρ_{fb}, divided by the guaranteed ultimate tensile strain, ε^*_{fu}

$$r_{\rho,d} = \frac{\rho_f}{\rho_{fb,d}\varepsilon_{fu}} \tag{2a}$$

and

$$r_\rho = \frac{\rho_f}{\rho_{fb}\varepsilon^*_{fu}} \tag{2b}$$

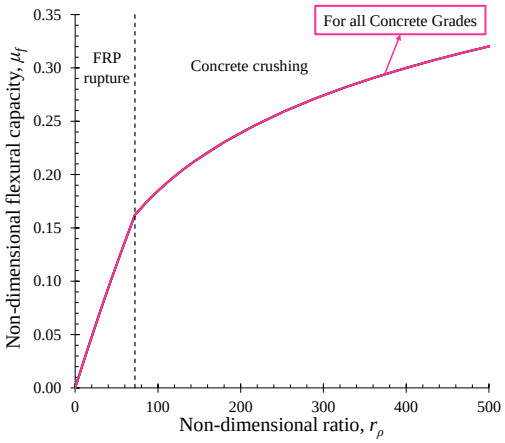

(a) Chart for ε^*_{fu}=0.0138 (for all concrete grades)

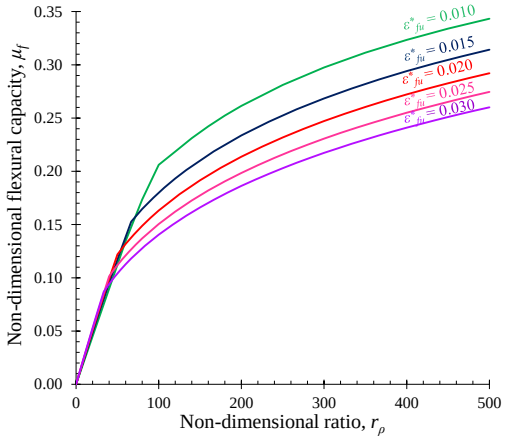

(b) General chart for various FRP materials

Fig. 2 Charts for the evaluation of the flexural capacity of concrete beams reinforced with FRP bars (without safety factors)

where the tensional reinforcement ratio, ρ_f, and the balanced FRP reinforcement ratio, $\rho_{fb,d}$ for design and ρ_{fb} for analysis (without safety factors), can be calculated as follows

$$\rho_f = \frac{A_f}{bd} \tag{3}$$

$$\rho_{fb,d} = 0.85\beta_1 \frac{f_c}{f_{fu}} \frac{E_f \varepsilon_c}{E_f \varepsilon_c + f_{fu}} \tag{4a}$$

$$\rho_{fb} = \frac{f_c}{f^*_{fu}} \frac{E_f \varepsilon_c}{E_f \varepsilon_c + f^*_{fu}} \tag{4b}$$

The curves illustrated in Fig. 1(a) were plotted for various concrete grades (from 20 to 60 MPa) and for specific (typical) material properties of the FRP bars: f_{fu}=f^*_{fu}=1800 MPa and ε_{fu}=ε^*_{fu}=0.0138. From the comparison of these curves it is obvious that the influence of the concrete grade is insignificant since the differences between the design curves in Fig. 1(a) for concrete grades from 20 to 60 MPa can be considered as negligible. This is due to the use of the non-dimensional variables in the specially developed charts. In Fig. 2(a) there is only one curve, common for all concrete grades since the reduction factors are omitted.

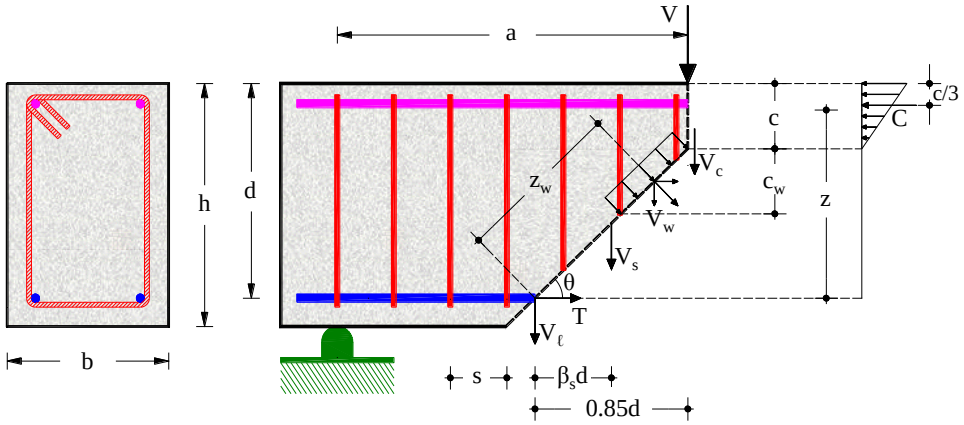

Fig. 3 Shear transfer mechanisms

The developed general charts for (i) design (Fig. 1(b)) and (ii) analysis without safety factors (Fig. 2(b)) include a series of curves based on the value of ε_{fu} and ε^*_{fu}, respectively. They can be used for various material properties of the composite reinforcing bars since ε_{fu} and ε^*_{fu} depend on the ultimate tensile strength and the modulus of elasticity of the FRP bars, as explained below. According to the provisions of ACI 440.1R-15, the balanced reinforcement ratio depends only on the properties of the concrete and the FRP bars (see also Eqs. 2(a) and (b)) and it has an important role for the estimation of the expected failure mode. Hence, taking the ratio of the reinforcement ratio, ρ_f, to the balanced ratio, ρ_{fb}, divided by the design tensile strain of the FRP, ε_{fu}, for design purposes or by the guaranteed ultimate tensile strain, ε^*_{fu}, for analysis, the tensile strength and the modulus of elasticity of the selected FRP material are taken into account and the charts in Figs. 1(b) and 2(b) can be used for various FRP material properties

$$\varepsilon^*_{fu} = \frac{f^*_{fu}}{E_f} \tag{5}$$

$$\varepsilon_{fu} = C_E \varepsilon^*_{fu} \tag{6}$$

In this way, based on the calculated design tensile strain of the selected FRP bar, ε_{fu}, the appropriate curve of the design general chart (Fig. 1(b)) is chosen and in conjunction with the value of the non-dimensional design bending moment, $\mu_{fd,\beta 1}$, using expression (1a) on the vertical axis of Fig. 1(b) the non-dimensional design ratio, $r_{\rho,d}$, on the horizontal axis can be determined. Consequently, the required reinforcement ratio of the examined beam can be calculated using expression (2a).

Likewise, the flexural strength of a beam can be estimated using the general chart of Fig. 2(b). Based on the provided reinforcement ratio of the FRP bars, the non-dimensional ratio, r_ρ (Eq. (2b)) on the horizontal axis can be calculated and in conjunction with the selected curve of the general chart, the value of the non-dimensional flexural capacity, μ_f, on the vertical axis in Fig. 2(b) can be estimate. The flexural strength, M_f, of the examined beam is then calculated using expression (1b).

2.2 Shear strength

For the evaluation of the shear capacity of the beams reinforced with longitudinal FRP bars with or without steel stirrups a combination of three theoretical considerations proposed by Oller *et al.* (2015) and Marí *et al.* (2014, 2015) has been adopted. It is noted that these models concern (i) concrete beams reinforced with FRP bars and FRP stirrups (Oller *et al.* 2015), (ii) concrete beams reinforced only with longitudinal FRP bars without transverse shear reinforcement (Marí *et al.* 2014) and (iii) conventionally RC beams with steel bars and steel stirrups (Marí *et al.* 2015). Fig. 3 demonstrates the shear transfer mechanisms in concrete beams reinforced with longitudinal FRP bars and conventional steel stirrups. It can be considered that the shear forces are resisted by the contribution of the un-cracked concrete chord, V_c, the transverse shear steel reinforcement crossing the critical diagonal crack, V_s, the tensile stresses transferred along the crack, V_w, depending on its width, and the shear transferred by the longitudinal FRP reinforcement, V_ℓ. Therefore, the calculation of the ultimate shear strength, V_f, is achieved using the sum

$$V_f = V_c + V_w + V_s + V_\ell \tag{7}$$

- Contribution of the un-cracked concrete chord, V_c

$$V_c = \zeta\left(1.072 - 0.01\alpha_e\right)\times \\ \times\left[\left(0.903 + 0.26\mu^*\right)\xi + 0.012 + 0.1325\mu^*\right] f_{ct} bd \tag{8}$$

where ζ is the size effect coefficient: ζ=1.2–0.2 a≥0.65 (α is the shear span in m) according to Zararis and Papadakis (2001); ξ is the neutral axis depth ratio and μ^* is the non-dimensional moment calculated by the expressions

$$\xi = \frac{c}{d} = \alpha_e \rho_f \left(-1 + \sqrt{1 + \frac{2}{\alpha_e \rho_f}}\right) \tag{9}$$

$$\mu^* = \mu + \beta_w \frac{V_w}{f_{ct} bd} + \beta_s \frac{V_s}{f_{ct} bd} \tag{10}$$

where μ is the non-dimensional cracking moment of the section where the critical shear crack initiates and is taken conservatively equal to 0.2 (Oller *et al.* 2015, Marí *et al.*

2015); β_s=0.85/2 since the shear force component of the steel reinforcement should be taken in the middle of the horizontal projection of the critical shear crack (see also Fig. 3, Marí *et al.* 2015) and β_w (Oller *et al.* 2015)

$$\beta_w = \frac{0.85 - 0.5\frac{c_w}{d}\cot\theta}{\cos^2\theta} \tag{11}$$

where c_w is the vertical projection of the crack length where the tensile stresses are extended (see also Fig. 3, Oller *et al.* 2015, Marí *et al.* 2015)

$$c_w = (d - c)\frac{\varepsilon_{ct,u}}{\varepsilon_r}\sin^2\theta \tag{12}$$

The ultimate tensile strain of concrete, $\varepsilon_{ct,u}$, is calculated according to Oller *et al.* (2015) and Marí *et al.* (2015) as

$$\varepsilon_{ct,u} = \frac{f_{ct}}{E_c}\left(1 + \frac{2G_f E_c}{f_{ct}^2 s_{m\theta}}\right) \tag{13}$$

where $s_{m\theta}$ is the average crack spacing of the inclined cracks (Oller *et al.* 2015)

$$s_{m\theta} = \frac{d - c}{2}\cos\theta \tag{14}$$

- *Shear force resisted along the critical crack, V_w (present study, Oller et al. 2015, Marí et al. 2015, Said et al. 2016)*

$$V_w = 0.425\frac{f_{ct}^2}{E_c\varepsilon_r}\sin^2\theta\left(1 + \frac{2G_f E_c}{f_{ct}^2 s_{m\theta}}\right)bd \xrightarrow{\varepsilon_r = 0.01}$$
$$V_w = 42.5\frac{f_{ct}^2}{E_c}\sin^2\theta\left(1 + \frac{2G_f E_c}{f_{ct}^2 s_{m\theta}}\right)bd \tag{15}$$

where: $G_f = 0.028 f_c^{0.18} d_{\max}^{0.32}$ (N/mm) is the fracture energy of concrete.

It is noted that the modulus of elasticity of the FRP bars is considerably lower than that of the steel bars. Said *et al.* (2016) observed that the strain of the tensional longitudinal FRP reinforcement, ε_r, when shear failure occurred were about 30 to 63% of the ultimate tensile strain, ε^*_{fu}, of the FRP bars. Therefore, in the present study the strain of the tensional longitudinal FRP reinforcement, ε_r, at shear failure is taken equal to 0.01.

- *Contribution of the steel transverse reinforcement, V_s (Marí et al. 2015)*

$$V_s = 0.85\rho_{sw} f_{yw} bd \tag{16}$$

- *Contribution of the longitudinal reinforcement, V_ℓ (Oller et al. 2015, Marí et al. 2015)*

$$V_\ell = 0.64 E_f A_f \frac{\varnothing_f^2 d}{s^3}\frac{\varepsilon_r}{1-\xi} \xrightarrow{\varepsilon_r = 0.01}$$
$$V_\ell = 0.0064 E_f A_f \frac{\varnothing_f^2 d}{s^3}\frac{1}{1-\xi} \tag{17}$$

Nevertheless, according to Oller *et al.* (2015) the contribution of the longitudinal FRP bars as dowel action to the ultimate shear strength is insignificant. Thus, to simplify the formulation of the ultimate shear strength the dowel action effect of the FRP bars could be neglected (V_ℓ=0). It is also noted that the rather complex expressions (7)-(17) for practising engineers could further be simplified by estimating the value of μ^* (and V_c) using available test data.

2.3 Flow chart and formulation

Figs. 4(a) and 4(b) demonstrate the flow chart of the calculation procedure according to the proposed methodology. As it is observed, after the estimation of the flexural capacity, M_f, and the shear strength, V_f, of the examined beam by using the proposed analytical models, the total strength, $P^M_{f,calc}$ and $P^V_{f,calc}$, which correspond to the flexural capacity, M_f, and shear strength, V_f, respectively, can be calculated as follows

$$P^M_{f,calc} = \frac{2M_f}{\mathrm{a}} \tag{18}$$

$$P^V_{f,calc} = 2V_f \tag{19}$$

It is obvious that expressions (18) and (19) can be applied only for beams with symmetrical concentrated point loads and for different loading conditions (such as beams with distributed loads) the relationships between M_f, V_f and P_f should be different. Nevertheless, in every case the shear span also expresses the ratio of the applied bending moment to the corresponding shear force: a = M_f / V_f.

Thus, the ultimate strength of the examined beam is

$$P_{tot,calc} = \min\left\{P^M_{f,calc}, P^V_{f,calc}\right\} \tag{20}$$

This way, the predicted failure mode of the beam can be estimated by comparing the calculated strengths due to flexure and shear, $P^M_{f,calc}$ and $P^V_{f,calc}$, respectively (see also Fig. 4(b)):

- If $P^M_{f,calc} < P^V_{f,calc}$ the expected failure mode is flexural with FRP rupture or concrete crushing.
- If $P^M_{f,calc} > P^V_{f,calc}$ the failure is governed by shear.

3. Experimental investigation

3.1 Test program

Two (2) RC beams with rectangular cross-section were designed and tested under four-point monotonic loading in order to acquire their experimental behaviour. The codified names of the examined beams are “F5.5” and “F10”. The beams have the same dimensions, the same high compressional steel reinforcement ratio in order to avoid premature failure of the compression zone of concrete and the same ratio of transverse reinforcement. Their total length is 2.7 m, the width to height ratio is *b/h*=200/250 mm, the effective depth is *d*=200 mm (see also Fig. 5), the shear span is a=1 m and the shear span-to-depth ratio is equal to a/*d*=5 (typical slender beams).

The compressional reinforcement consists of common

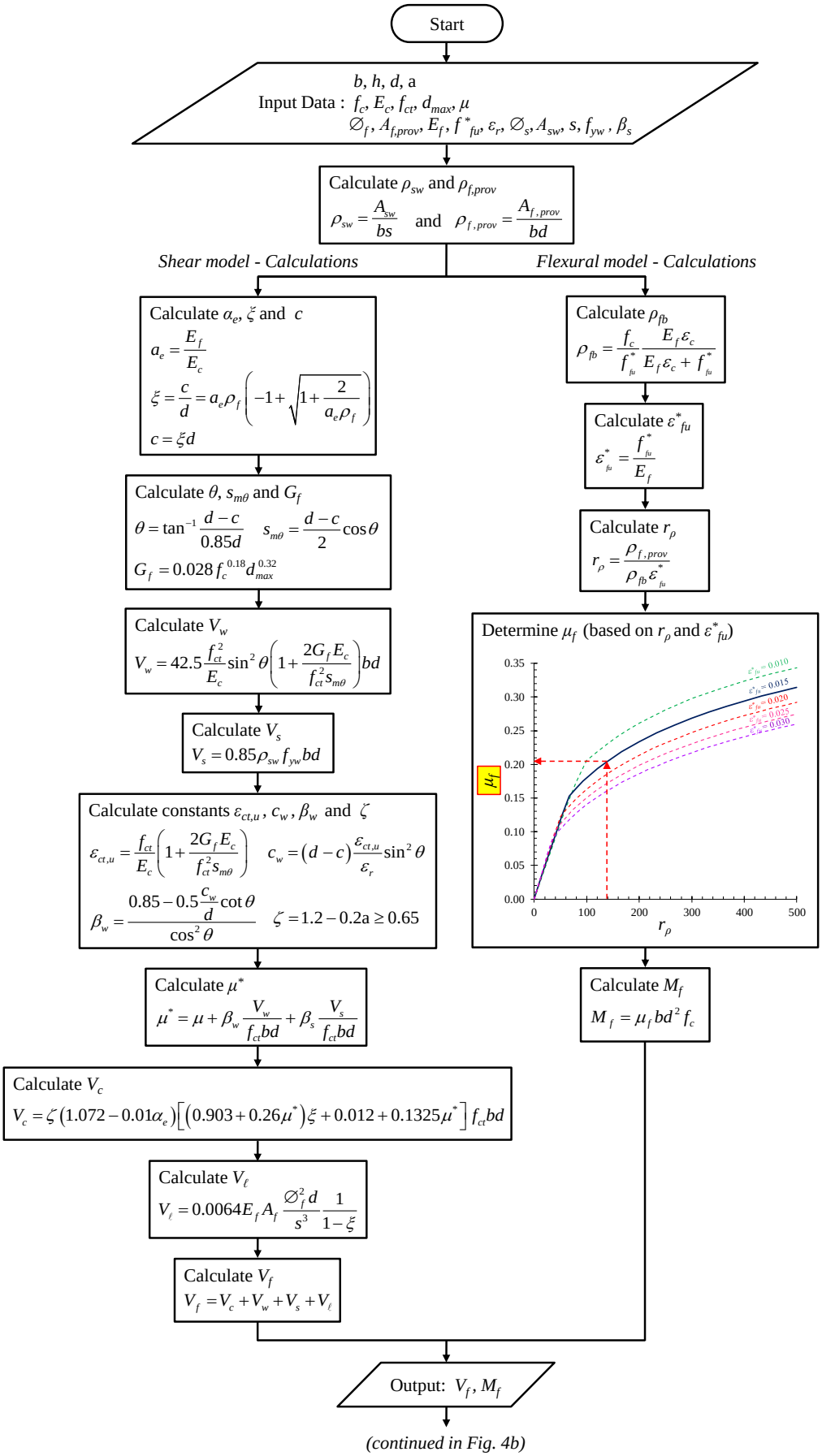

Fig. 4(a) Flow chart of the calculation procedure for concrete beams with longitudinal FRP bars – Part A

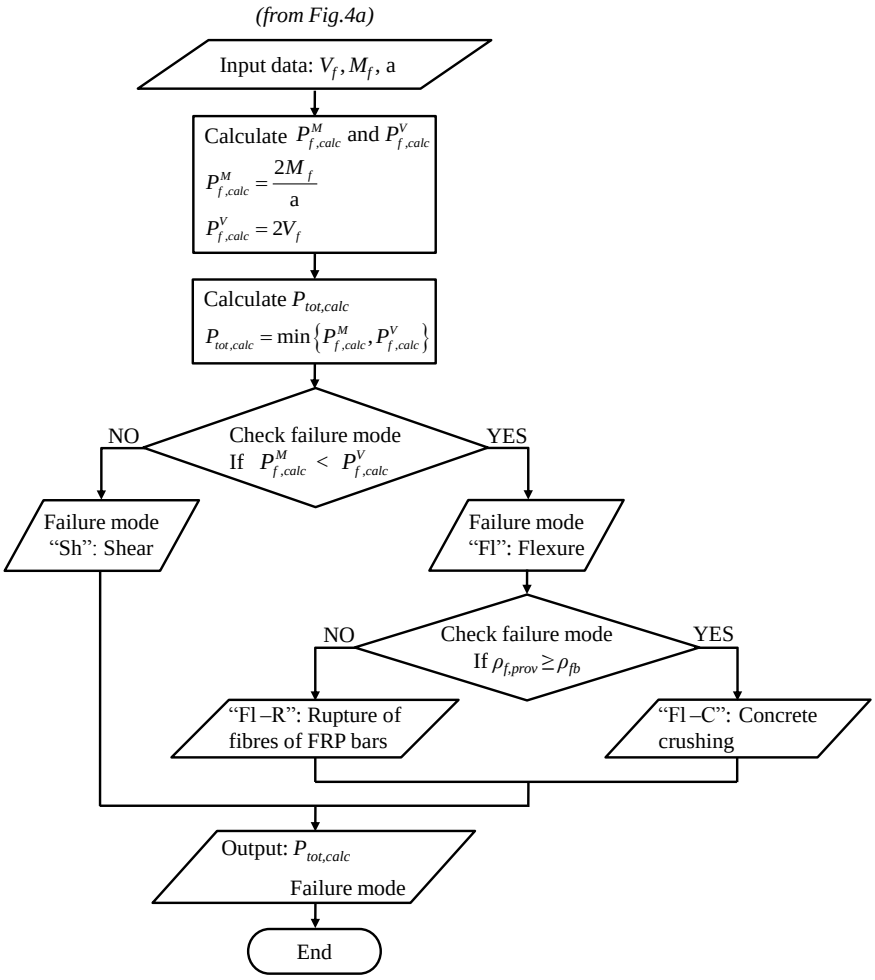

Fig. 4(b) Flow chart of the calculation procedure for concrete beams with longitudinal FRP bars – Part B

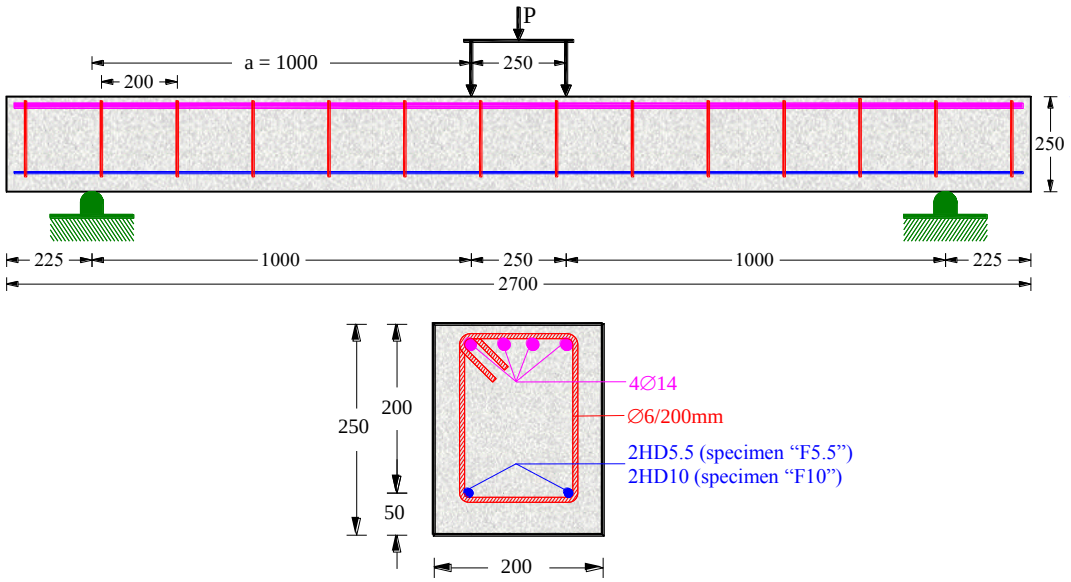

Fig. 5 Geometry and reinforcement details of the tested beams (dimensions in mm)

deformed steel bars of diameter 14 mm (4∅14 top) and the transverse shear reinforcement includes mild steel closed stirrups of diameter 6 mm spacing at 200 mm (∅6/200 mm). The ratio of the provided stirrups is low and rather inadequate in order to examine the case of prevailing shear failure. The yield tensile strength of the deformed steel bars and the mild steel stirrups are 550 MPa and 310 MPa, respectively.

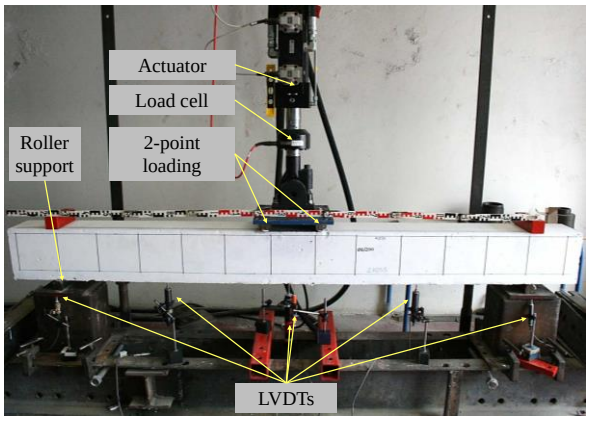

Fig. 6 Test rig and instrumentation

The tensional reinforcement of the beams "F5.5" and "F10" consists of two carbon FRP bars of diameter 5.5 mm (2HD5.5) and 10 mm (2HD10), respectively. The geometrical and the reinforcement characteristics of the beams are shown in Fig. 5 and Table 1a.

The diameter and the amount of the FRP bars were chosen according to the design guidelines of ACI 440.1R-15 (2015). The tensional reinforcement ratio, ρ_f, and the balanced FRP reinforcement ratio, $\rho_{fb,d}$, for design can be calculated using expressions (3) and (4a). The predicted failure mode can be determined by comparing the FRP tensional reinforcement ratio, ρ_f, to the design balanced FRP reinforcement ratio, $\rho_{fb,d}$: If $\rho_f < \rho_{fb,d}$, the beam is considered as under-reinforced and FRP rupture failure mode governs. Otherwise, if $\rho_f > \rho_{fb,d}$, the beam is considered as over-reinforced and the failure is expected to occur due to concrete crushing. The reinforcement ratio of the FRP bars of the beams "F5.5" and "F10" is 0.12 % and 0.39 %, respectively; whereas the design balanced reinforcement ratio is 0.21 %. Thus, according to ACI 440.1R-15 (2015) the tested beams "F5.5" is alleged as under-reinforced against flexure and the expected failure mode is flexural with FRP rupture. On the contrary, the beam "F10" is over-reinforced against flexure in the tensional zone, highly steel reinforced in the compression zone and slightly steel reinforced against shear, thus, shear failure due to concrete diagonal tension is expected.

The used carbon FRP bars (HD5.5 and HD10) were produced by the pultrusion process of the fibres according to the specifications of the manufacturer. The nominal ultimate tensile strength, f_{fu}, and the elastic modulus, E_f, of carbon FRP bars are 1.8 GPa and 130 GPa, respectively. Standard concrete cylinders of 150×300 mm were tested by compression and splitting tests at the day of the tests. The mean values of the cylinder compressive strength and the splitting tensile strength of the used concrete of all beams are 29.1 MPa and 2.42 MPa, respectively. The maximum aggregate size of concrete is 16 mm.

A typical four-point bending scheme and setup is adopted for the monotonic loading of the RC beams, as presented in Fig. 6. Tested beams were simply edge-supported on a rigid laboratory frame using roller supports 2.25 m apart. The imposed load was applied in two points 250 mm apart in the mid-span of the beams (four points loading). The width of the supporting and the loading plates is 30 mm. The length of the shear span of the beams is a=1 m and the span-to-depth ratio is a/*d*=5 (typical slender beam).

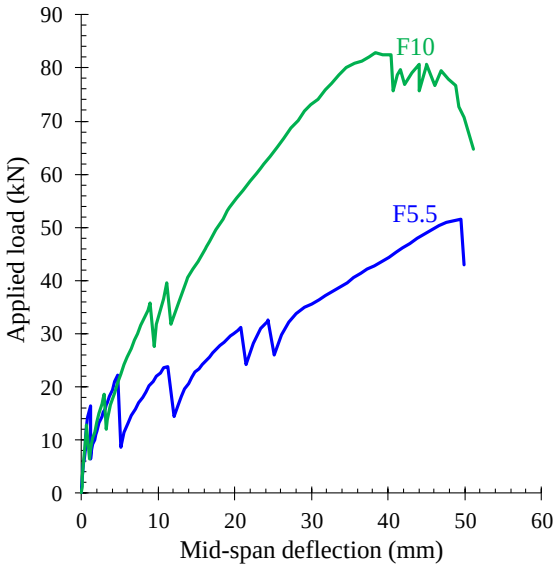

(a) Applied load vs mid-span deflection curves

(b) "F5.5": Beam with FRP bars 5.5 mm (flexural failure due to FRP rupture)

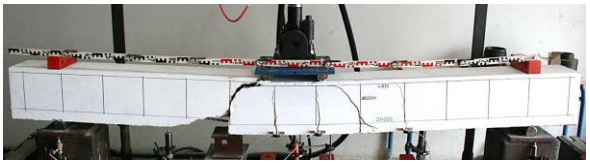

(c) "F10": Beam with FRP bars 10 mm (shear failure)

Fig. 7 Experimental behaviour of the tested beams and photographs at failure

The imposed load was consistently increased with low rate using a pinned-end actuator and was measured by a load cell with accuracy equal to 0.05 kN. The deflections of the tested beams were recorded using measurements of six Linear Variable Differential Transducers (LVDTs). Two of the installed LVDTs were placed at the mid-span of the beams (one at the front side and one at the back side to increase accuracy), one at the middle of the left shear span, one at the middle of the left shear span and two at the supports (see also Fig. 6). This way, the net deflections at the mid-span and at the middle of the left-span and of the right-span of the beams were accurately estimated.

The experimental behaviour of the tested beams is demonstrated in Fig. 7(a) in terms of the applied load versus mid-span deflection curves. It is observed that the experimental curves demonstrate significant fluctuations with sudden-rapid reduction of the applied load after each crack formation and subsequent increases until the next crack ("saw-tooth shaped" response curves). In particular

when the applied moment initially reached the cracking strength, a first flexural crack appeared at the region of the constant maximum moment or nearby this region. Then, the applied load reduced instantly. As the test proceeded the applied load increased with decreased stiffness as indicated from the reduced slope of the curves presented in Fig. 7(a). Whenever a subsequent new crack appeared, the load rapidly reduced and the already existing cracks closed. It is stressed that similar behaviour has also been observed in the monotonic tests of concrete beams with glass FRP bars in the recent studies of Goldston *et al.* (2016, 2017).

The typical failure modes of the tested beams "F5.5" with 2HD5.5 and "F10" with 2HD10 carbon FRP bars are illustrated in Fig. 7(b) and (c), respectively. Fig. 7(b) illustrates the cracking pattern at failure of the under-reinforced beam "F5.5". It is observed that only a few deep and wide flexure cracks were formed. The beam failed due to the rupture of the carbon fibres of the FRP bars (HD5.5), as it was designed and expected according to ACI 440.1R-15 (2015). Fig. 7(c) presents the cracking pattern at failure of the over-reinforced beam "F10" and concrete crushing instead of FRP rupture is expected according to ACI 440.1R-15 (2015). As it is illustrated in Fig. 7(c), the observed failure of the beam "F10" is governed by shear due to the low ratio of the shear reinforcement and the highly reinforced compression zone. Therefore, at high level of the applied load some of the initially formed flexural cracks gradually demonstrated a shear-diagonal character. As the applied load further increased a dowel action of the FRP bars has also been developed and the critical diagonal crack became wider. Consequently, as high vertical tensile stresses develop in the surrounding concrete at the level of the longitudinal bars, concrete cover spalling failure along the FRP bars has been occurred. Eventually, due to the low ratio of the shear reinforcement and the relatively low strength, diameter and stiffness of the FRP bars in the transverse direction, typical shear failure due to concrete diagonal tensional failure finally occurred. From the cracking patterns of beams "F5.5" and "F10" illustrated in Fig. 7 (b) and (c), respectively, only a few concrete cracks are observed. Further, the critical shear crack in beam "F10" is very close to the imposed load point. These observations indicate the poor bonding properties of the used FRP bars. A summary of the experimental results of the beams is also given in Table 1a.

3.2 Experimental database

The proposed analytical approach described in the flow chart in Figs. 4(a) and 4(b) has been applied to 138 typical slender beams with a/*d*>2.5 in order to establish the validity of the developed methodology. The database of the experimental information is compiled from 13 existing works of the literature (Masmoudi *et al*. 1998, Toutanji and Saafi 2000, Yost *et al*. 2001, Ashour 2006, Rafi *et al*. 2008, Shin *et al*. 2009, Barris *et al*. 2009, Lee and Kim *et al*. 2012, Kim and Jang 2013, Refai *et al*. 2015, Zhang *et al*. 2015, Ovitigala *et al*. 2016, Elgabbas *et al*. 2017). All these tests are beam specimens subjected to monotonic loading using a four-point bending scheme. The used database includes under- and over-reinforced beams with four different types of FRP bars (bars made of Aramid, Basalt, Carbon or Glass fibres). It is noted that the shear-dominated beams (Yost *et al*. 2001, Ashour *et al*. 2006, Kim and Jang 2013) have no transverse reinforcement.

Tables 1 a-f present the geometrical, the mechanical and the reinforcement characteristics along with the experimental data of the tested beams selected from the literature, as well as the calculations derived from the proposed analytical approach. These calculations are:

- The non-dimensional ratio, r_ρ, and the calculated flexural strength, $M_{f,prop}$, as derived from expressions (2b) and (1b), respectively, according to the proposed general chart in Fig. 2(b).
- The calculated shear strength, $V_{f,prop}$, as derived from expression (7) according the proposed model.
- The calculated total strength, $P^M_{f,calc}$ *and* $P^V_{f,calc}$, which correspond to the calculated flexural, $M_{f,prop}$, and shear strength, $V_{f,prop}$, respectively, according to the proposed methodology.
- The ratio of the ultimate experimental applied load, $P_{tot,exp}$, to the calculated one, $P_{tot,calc}$, in order to check the accuracy of the developed methodology.
- The predicted failure mode based on the proposed procedure shown in the flow chart of Figs. 4(a) and 4(b) compared to the experimentally observed failure mode.

3.3 Comparisons between test and analytical results

From the comparison between the experimental data and the analytically predicted ultimate strength and failure mode, as they derived from the proposed procedure, it is concluded that in the majority of the examined cases a good agreement is achieved (see also Tables 1 a-f). Only in 5 from the 138 examined beams (or in a 4 % of the total) there is a rather significant discrepancy between the experimental and the calculated ultimate strength of the beam specimens and only in 7 of them there is a difference between the experimentally observed and the predicted failure mode. It is stressed that all three different failure modes; (i) concrete crushing, (ii) FRP rupture or (iii) shear failure can be predicted using the proposed analytical approach.

Further, in Fig. 8 the analytical predictions of the ultimate strength calculated from the proposed methodology, $P_{tot,calc}$, are illustrated versus the corresponding strength derived from the tests, $P_{tot,exp}$, for all the 138 examined beams. A satisfactory accuracy is confirmed since the mean value of the ratio $P_{tot,exp}/P_{tot,calc}$ is 1.028 with standard deviation 12.7%. Especially, for the examined beams predicted to fail in flexure the mean value of $P_{tot,exp}/P_{tot,calc}$ is 1.034 with standard deviation 13.4%, whereas for the beams predicted to fail in shear the mean value of this ratio is 1.020 with standard deviation 11.7%.

4. Numerical example

The flexural and the shear strength of the shear-dominated beam "F10" (present study) are calculated. The geometrical and reinforcement characteristics of the examined beam are shown in Fig. 5.

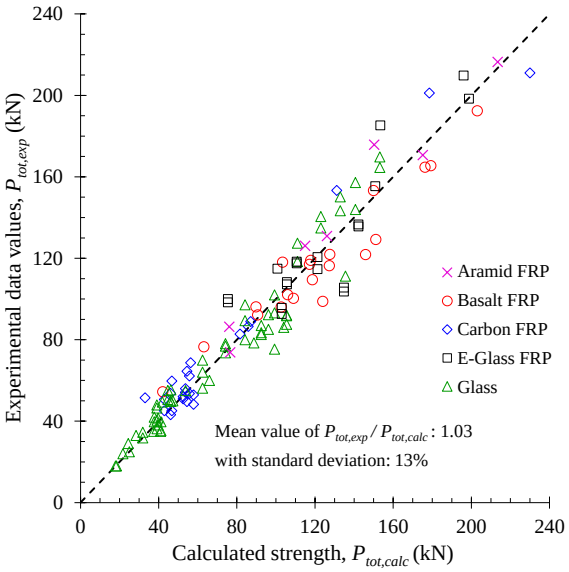

Fig. 8 Experimental data versus analytical results from 138 beams of the present study and the literature

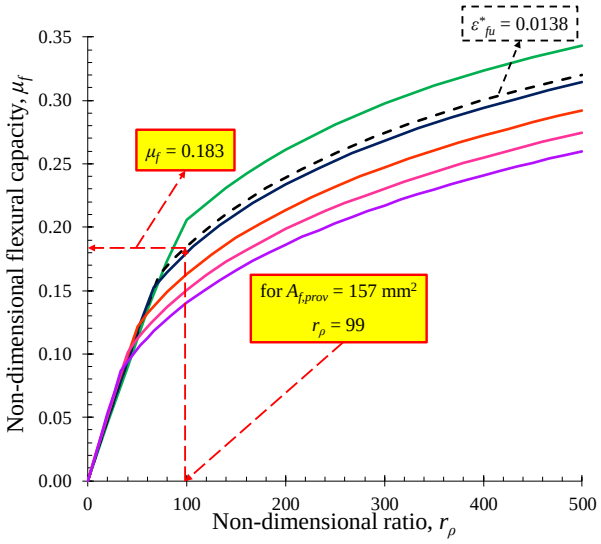

Fig. 9 Evaluation of the flexural capacity of the examined beam (without safety factors)

4.1 Flexural strength

- *Data of the beam "F10" (present study):* The examined beam specimen has rectangular cross-section with dimensions *b/h*=200/250 mm, effective depth *d*=200 mm and two tensional carbon FRP bars of diameter 10 mm (A_f=157 mm^2) with guaranteed ultimate flexural strength f^*_{fu}=1800 MPa and modulus of elasticity E_f=130 GPa (see also Fig. 5). The measured mean concrete cylinder compressive strength is f_c=29.1 MPa.

- *Ultimate tensile strain of the provided FRP bars:*

$$\varepsilon^*_{fu} = \frac{f^*_{fu}}{E_f} = \frac{1800}{130\times10^6} = 1.38\,\%$$

- *Reinforcement ratio of the provided FRP bars, $\rho_{f,prov}$, and balanced ratio, ρ_{fb}:* They are calculated using expressions (3) and (4a), respectively:

$$\rho_{f,prov} = \frac{A_{f,prov}}{bd} = \frac{157}{200\times200} = 0.393\,\%$$

$$\rho_{fb} = \frac{f_c}{f^*_{fu}}\frac{E_f\varepsilon_c}{E_f\varepsilon_c + f^*_{fu}} \rightarrow$$

$$\rho_{fb} = \frac{29.1}{1800}\frac{130{,}000\times0.003}{130{,}000\times0.003+1800} = 0.288\,\%$$

- *Non-dimensional ratio, r_ρ:* It is calculated using expression (2b):

$$r_\rho = \frac{\rho_f}{\rho_{fb}\varepsilon^*_{fu}} = \frac{0.00393}{0.00288\times0.0138} = 99$$

- *Non-dimensional flexural capacity, μ_f, using the developed general chart:* According to the material properties of the provided FRP bars (ε^*_{fu}=1.38%) the appropriate curve of the develop general chart (Fig. 2(b)) is chosen and in conjunction with the non-dimensional ratio (r_ρ=99) on the horizontal axis it is concluded that the non-dimensional flexural capacity, μ_f, on the vertical axis is equal to μ_f=0.183. The procedure is also illustrated with details in Fig. 9.

- *Flexural capacity, M_f:* It is calculated using expression (1b):

$$M_f = \mu_f bd^2 f_c \rightarrow$$

$$M_f = 0.183\times200\times200^2\times29.1\times10^{-6} = 42.6\ \text{kNm}$$

- *Total strength in terms of applied load, $P^M_{f,calc}$, which corresponds to the flexural capacity, M_f:* It is calculated using expression (18):

$$P^M_{f,calc} = \frac{2M_f}{\text{a}} = \frac{2\times42.6}{1} = 85.2\ \text{kN}$$

4.2 Shear strength

- *Data of the shear-dominated beam"F10" (present study):* The examined beam has cross-sectional dimensions *b/h*=200/250 mm, effective depth *d*=200 mm and two tensional carbon FRP bars of diameter 10 mm (A_f=157 mm^2) with guaranteed ultimate flexural strength f^*_{fu}=1800 MPa and elastic modulus E_f=130 GPa. Mild steel closed stirrups of diameter 6 mm spacing at 200 mm (∅6/200 mm) with yield tensile strength f_{yw}=310 MPa consist the steel transverse reinforcement. The mean concrete cylinder compressive strength is f_c=29.1 MPa, the splitting tensile strength is $f_{ct,spl}$=2.42 MPa and the concrete maximum aggregate size is d_{max}=16 mm. The shear span is a=1 m (see also Fig. 5).

- *Mechanical properties of concrete:* Tensile concrete strength, f_{ct}, elastic modulus, E_c, and fracture of energy, G_f:

$$f_{ct} = f_{ct.spl} = 2.42\ \text{MPa}$$

$$E_c = 22\left(\frac{f_c}{10}\right)^{0.3} = 22\times\left(\frac{29.1}{10}\right)^{0.3} = 30\ \text{GPa}$$

$$G_f = 0.028\,f_c^{0.18}d_{\max}^{0.32} \rightarrow$$

$$G_f = 0.028\times29.1^{0.18}\times16^{0.32} = 0.125\ \text{N/mm}^2$$

- *Characteristics of the longitudinal and the shear transverse reinforcement:* The longitudinal FRP bars ratio, ρ_f, and the steel stirrups ratio, ρ_{sw}, are:

Table 1a Test data and analytical predictions of the examined beams from the present study and the literature

Beam codified name	Geometrical properties				Material properties				FRP reinforcement					Stirrups				Experimental results			Analytical results (according to the proposed model)										Failure mode	
	b (mm)	h (mm)	d (mm)	a/d	f_c (MPa)	f^*_{fu} (MPa)	E_f (GPa)	ε^*_{fu} (%)	FRP type	No	$\varnothing_f$ (mm)	A_f (mm^2)	$\rho_{f,exp}$ (%)	ρ_{fb} (%)	$\varnothing_s$ (mm)	s (mm)	ρ_{sw} (%)	f_{yw} (MPa)	$P_{tot,exp}$ (kN)	V_{exp} (kN)	M_{exp} (kNm)	r_ρ	μ_f	$M_{f,prop}$ (kNm)	$V_{f,prop}$ (kN)	$P^M_{f,calc}$ (kN)		$P^V_{f,calc}$ (kN)	$P_{tot,calc}$ (kN)	$\frac{P_{tot,exp}}{P_{tot,calc}}$	Obs. Fail.	Pred. Fail.
Present studt																																
F5.5	200	250	200	5.0	29.1	1800	130	1.38	C	2	5.5	48	0.12	0.29	6	200	0.14	310	52	26	25.8	30	0.071	16.5	33.2	33.1	<	66.3	33.1	1.56	Fl-R	Fl-R
F10	200	250	200	5.0	29.1	1800	130	1.38		2	10	157	0.39	0.29	6	200	0.14	310	83	41	41.4	99	0.183	42.6	40.8	85.2	>	81.6	81.6	1.01	Sh	Sh
Masmoudi *et al.* (1998)																																
CB2B-1	200	300	253	4.9	52.0	773	38	2.06	E-G	2	14.9	349	0.69	0.86	10	80	0.98	480	93	46	57.9	39	0.097	64.3	257.3	102.9	<	514.7	102.9	0.90	Fl-C	Fl-R
CB2B-2	200	300	253	4.9	52.0	773	38	2.06		2	14.9	349	0.69	0.86	10	80	0.98	480	96	48	59.8	39	0.097	64.3	257.3	102.9	<	514.7	102.9	0.93	Fl-C	Fl-R
CB3B-1	200	300	253	4.9	52.0	773	38	2.06		3	14.9	523	1.04	0.86	10	80	0.98	480	106	53	66.0	59	0.127	84.2	267.7	134.8	<	535.3	134.8	0.78	Fl-C	Fl-C
CB3B-2	200	300	253	4.9	52.0	773	38	2.06		3	14.9	523	1.04	0.86	10	80	0.98	480	104	52	64.8	59	0.127	84.2	267.7	134.8	<	535.5	134.8	0.77	Fl-C	Fl-C
CB4B-1	200	300	230	5.4	45.0	773	38	2.06		4	14.9	697	1.52	0.74	10	80	0.98	480	121	60	75.4	99	0.159	75.8	255.0	121.2	<	510.0	121.2	1.00	Fl-C	Fl-C
CB4B-2	200	300	230	5.4	45.0	773	38	2.06		4	14.9	697	1.52	0.74	10	80	0.98	480	115	57	71.7	99	0.159	75.8	255.0	121.2	<	510.0	121.2	0.95	Fl-C	Fl-C
CB6B-1	200	300	230	5.4	45.0	773	38	2.06		6	14.9	1046	2.27	0.74	10	80	0.98	480	136	68	84.8	149	0.187	88.9	272.1	142.2	<	544.2	142.2	0.95	Fl-C	Fl-C
CB6B-2	200	300	230	5.4	45.0	773	38	2.06		6	14.9	1046	2.7	0.74	10	80	0.98	480	137	68	85.4	149	0.187	88.9	272.1	142.2	<	544.2	142.2	0.96	Fl-C	Fl-C
Toutanji and Saafi (2000)																																
GB1-1	180	300	268	4.5	35.0	695	40	1.74	E-G	2	12.7	253	0.53	0.74	9.5	100	0.79	460	100	50	60.0	41	0.100	45.2	187.3	75.4	<	374.6	75.4	1.33	Fl-C	Fl-R
GB1-2	180	300	268	4.5	35.0	695	40	1.74		2	12.7	253	0.53	0.74	9.5	100	0.79	460	98	49	59.0	41	0.100	45.2	187.3	75.4	<	374.6	75.4	1.30	Fl-C	Fl-R
GB2-1	180	300	268	4.5	35.0	695	40	1.74		3	12.7	380	0.79	0.74	9.5	100	0.79	460	108	54	65.0	61	0.140	63.3	192.7	105.6	<	385.3	105.6	1.03	Fl-C	Fl-C
GB2-2	180	300	268	4.5	35.0	695	40	1.74		3	12.7	380	0.79	0.74	9.5	100	0.79	460	107	54	64.3	61	0.140	63.3	192.7	105.6	<	385.3	105.6	1.02	Fl-C	Fl-C
GB3-1	180	300	255	4.7	35.0	695	40	1.74		4	12.7	507	1.10	0.74	9.5	100	0.79	460	118	59	71.0	86	0.162	66.4	188.6	110.6	<	377.1	110.6	1.07	Fl-C	Fl-C
GB3-2	180	300	255	4.7	35.0	695	40	1.74		4	12.7	507	1.10	0.74	9.5	100	0.79	460	118	59	70.5	86	0.162	66.4	188.6	110.6	<	377.1	110.6	1.06	Fl-C	Fl-C
Yost *et al.* (2001)																																
1FRP[a]	229	286	225	4.1	36.3	690	40	1.71	G	2	19.1	570	1.11	0.79	-	-	-	-	78	39	35.7	82	0.160	67.3	37.1	147.3	>	74.2	74.2	1.05	Sh	Sh
1FRP[b]	229	286	225	4.1	36.3	690	40	1.71		2	19.1	570	1.11	0.79	-	-	-	-	77	38	35.1	82	0.160	67.3	37.1	147.3	>	74.2	74.2	1.04	Sh	Sh
1FRP[c]	229	286	225	4.1	36.3	690	40	1.71		2	19.1	570	1.11	0.79	-	-	-	-	74	37	33.6	82	0.160	67.3	37.1	147.3	>	74.2	74.2	0.99	Sh	Sh
2FRP[a]	178	286	225	4.1	36.3	690	40	1.71		2	19.1	570	1.42	0.79	-	-	-	-	56	28	25.7	106	0.176	57.6	31.2	126.0	>	62.4	62.4	0.90	Sh	Sh
2FRP[b]	178	286	225	4.1	36.3	690	40	1.71		2	19.1	570	1.42	0.79	-	-	-	-	70	35	32.0	106	0.176	57.6	31.2	126.0	>	62.4	62.4	1.12	Sh	Sh
2FRP[c]	178	286	225	4.1	36.3	690	40	1.71		2	19.1	570	1.42	0.79	-	-	-	-	64	32	29.3	106	0.176	57.6	31.2	126.0	>	62.4	62.4	1.03	Sh	Sh
3FRP[a]	229	286	225	4.1	36.3	690	40	1.71		3	19.1	855	1.66	0.79	-	-	-	-	80	40	36.6	124	0.188	79.1	42.1	173.1	>	84.2	84.2	0.95	Sh	Sh

Notation of FRP types: A: Aramid, B: Basalt, C: Carbon, E-G: Glass fibres with higher electrical resistivity and G: Glass
Notation of failure modes: Fl-R: Rupture of fibres of bars, Fl-C: Concrete Crushing and Sh: Diagonal shear failure

Table 1b Test data and analytical predictions of the examined beams from the present study and the literature

Beam codified name	Geometrical properties				Material properties				FRP reinforcement					Stirrups				Experimental results					Analytical results (according to the proposed model)									Failure mode	
	b (mm)	h (mm)	d (mm)	a/d	f_c (MPa)	f^*_{fu} (MPa)	E_f (GPa)	ε^*_{fu} (%)	FRP type	No	$\varnothing_f$ (mm)	A_f (mm^2)	$\rho_{f,exp}$ (%)	ρ_{fb} (%)	$\varnothing_s$ (mm)	s (mm)	ρ_{sw} (%)	f_{yw} (MPa)	$P_{tot,exp}$ (kN)	V_{exp} (kN)	M_{exp} (kNm)	r_ρ	μ_f	$M_{f,prop}$ (kNm)	$V_{f,prop}$ (kN)	$P^M_{f,calc}$ (kN)		$P^V_{f,calc}$ (kN)	$P_{tot,calc}$ (kN)	$\frac{P_{tot,exp}}{P_{tot,calc}}$	Obs. Fail.	Pred. Fail.
Yost *et al.* (2001) *(continued)*																																
3FRP[b]	229	286	225	4.1	36.3	690	40	1.71		3	19.1	855	1.66	0.79	-	-	-	-	97	49	44.4	124	0.188	79.1	42.1	173.1	>	84.2	84.2	1.15	Sh	Sh
3FRP[c]	229	286	225	4.1	36.3	690	40	1.71		3	19.1	855	1.66	0.79	-	-	-	-	89	45	40.9	124	0.188	79.1	42.1	173.1	>	84.2	84.2	1.06	Sh	Sh
4FRP[a]	279	286	225	4.1	36.3	690	40	1.71		4	19.1	1140	1.82	0.79	-	-	-	-	88	44	40.0	135	0.193	99.0	52.7	216.5	>	105.5	105.5	0.83	Sh	Sh
4FRP[b]	279	286	225	4.1	36.3	690	40	1.71		4	19.1	1140	1.82	0.79	-	-	-	-	92	46	42.0	135	0.193	99.0	52.7	216.5	>	105.5	105.5	0.87	Sh	Sh
4FRP[c]	279	286	225	4.1	36.3	690	40	1.71		4	19.1	1140	1.82	0.79	-	-	-	-	92	46	42.1	135	0.193	99.0	52.7	216.5	>	105.5	105.5	0.87	Sh	Sh
5FRP[a]	254	286	224	4.1	36.3	690	40	1.71	E-G	3	22.2	1164	2.05	0.79	-	-	-	-	75	38	34.5	152	0.200	92.5	49.6	202.5	>	99.3	99.3	0.76	Sh	Sh
5FRP[b]	254	286	224	4.1	36.3	690	40	1.71		3	22.2	1164	2.05	0.79	-	-	-	-	102	51	46.6	152	0.200	92.5	49.6	202.5	>	99.3	99.3	1.03	Sh	Sh
5FRP[c]	254	286	224	4.1	36.3	690	40	1.71		3	22.2	1164	2.05	0.79	-	-	-	-	93	47	42.6	152	0.200	92.5	49.6	202.5	>	99.3	99.3	0.94	Sh	Sh
6FRP[a]	229	286	224	4.1	36.3	690	40	1.71		3	22.2	1164	2.27	0.79	-	-	-	-	87	44	39.8	169	0.211	88.0	46.2	192.6	>	92.5	92.5	0.94	Sh	Sh
6FRP[b]	229	286	224	4.1	36.3	690	40	1.71		3	22.2	1164	2.27	0.79	-	-	-	-	84	42	38.2	169	0.211	88.0	46.2	192.6	>	92.5	92.5	0.90	Sh	Sh
6FRP[c]	229	286	224	4.1	36.3	690	40	1.71		3	22.2	1164	2.27	0.79	-	-	-	-	83	41	37.7	169	0.211	88.0	46.2	192.6	>	92.5	92.5	0.89	Sh	Sh
Ashour (2006)																																
Beam1	150	200	167	4.0	27.7	650	38	1.71		4	6	113	0.45	0.64	-	-	-	-	25	13	8.3	42	0.101	11.7	12.5	35.1	>	25.0	25.0	1.00	Sh	Sh
Beam2	150	200	167	4.0	27.7	650	38	1.71		2	6	57	0.23	0.64	-	-	-	-	18	9	6.0	21	0.053	6.1	10.6	18.4	<	21.1	18.4	0.98	Fl-R	Fl-R
Beam3	150	250	217	3.1	27.7	705	32	2.20		2	12	226	0.69	0.47	-	-	-	-	35	18	11.7	67	0.130	25.4	18.7	76.2	>	37.5	37.5	0.93	Sh	Sh
Beam4	150	250	217	3.1	27.7	650	38	1.71		2	6	57	0.17	0.64	-	-	-	-	24	12	8.0	16	0.037	7.2	13.6	21.7	<	27.1	21.7	1.11	Fl-R	Fl-R
Beam5	150	300	267	2.5	27.7	705	32	2.20		3	12	339	0.85	0.47	-	-	-	-	50	25	16.7	82	0.145	42.9	23.6	128.7	>	47.2	47.2	1.06	Sh	Sh
Beam6	150	300	267	2.5	27.7	650	38	1.71	G	2	6	57	0.14	0.64	-	-	-	-	33	17	11.0	13	0.032	9.5	15.2	28.4	>	30.4	28.4	1.16	Fl-R	Fl-R
Beam7	150	200	167	4.0	50.1	705	32	2.20		3	12	339	1.35	0.85	-	-	-	-	35	18	11.7	72	0.137	28.7	20.5	86.1	>	40.9	40.9	0.86	Sh	Sh
Beam8	150	200	167	4.0	50.1	650	38	1.71		2	6	57	0.23	1.15	-	-	-	-	18	9	6.0	11	0.029	6.0	13.2	17.9	<	26.5	17.9	1.00	Fl-R	Fl-R
Beam9	150	250	217	3.1	50.1	705	32	2.20		3	12	339	1.04	0.85	-	-	-	-	55	28	18.3	56	0.121	42.8	26.9	128.4	>	53.8	53.8	1.02	Sh	Sh
Beam10	150	250	217	3.1	50.1	650	38	1.71		2	6	57	0.17	1.15	-	-	-	-	29	15	9.7	9	0.023	8.1	17.3	24.4	<	34.5	24.4	1.19	Fl-R	Fl-R
Beam11	150	300	267	2.5	50.1	705	32	2.20		4	12	452	1.13	0.85	-	-	-	-	60	30	20.0	60	0.127	68.0	33.0	204.1	>	66.0	66.0	0.91	Sh	Sh
Beam12	150	300	267	2.5	50.1	650	38	1.71		4	6	113	0.28	1.15	-	-	-	-	50	25	16.7	14	0.036	19.3	23.1	57.8	>	46.1	46.1	1.08	Fl-R	Sh

Notation of FRP types: A: Aramid, B: Basalt, C: Carbon, E-G: Glass fibres with higher electrical resistivity and G: Glass
Notation of failure modes: Fl-R: Rupture of fibres of bars, Fl-C: Concrete Crushing and Sh: Diagonal shear failure

Table 1c Test data and analytical predictions of the examined beams from the present study and the literature

Beam codified name	Geometrical properties				Material properties				FRP reinforcement					Stirrups				Experimental results			Analytical results (according to the proposed model)										Failure mode	
	b (mm)	h (mm)	d (mm)	a/d	f_c (MPa)	f^*_{fu} (MPa)	E_f (GPa)	ε^*_{fu} (%)	FRP type	No	$\varnothing_f$ (mm)	A_f (mm^2)	$\rho_{f,exp}$ (%)	ρ_{fb} (%)	$\varnothing_s$ (mm)	s (mm)	ρ_{sw} (%)	f_{yw} (MPa)	$P_{tot,exp}$ (kN)	V_{exp} (kN)	M_{exp} (kNm)	r_ρ	μ_f	$M_{f,prop}$ (kNm)	$V_{f,prop}$ (kN)	$P^M_{f,calc}$ (kN)		$P^V_{f,calc}$ (kN)	$P_{tot,calc}$ (kN)	$\frac{P_{tot,exp}}{P_{tot,calc}}$	Obs. Fail.	Pred. Fail.
Rafi *et al.* (2008)																																
BRC1	120	200	169	4.0	42.6	1676	136	1.23	C	2	9.5	142	0.70	0.50	6	100	0.47	421	89	44	30.0	114	0.201	29.4	58.7	87.1	<	117.5	87.1	1.02	Fl-C	Fl-C
BRC2	120	200	169	4.0	41.7	1676	136	1.23		2	9.5	142	0.70	0.49	6	100	0.47	421	87	43	29.2	116	0.202	29.0	58.5	85.8	<	117.1	85.8	1.01	Fl-C	Fl-C
Shin *et al.* (2006)																																
FB-2	300	400	354	3.4	34.0	690	41	1.68	E-G	2	12.7	253	0.24	0.75	9.5	171	0.28	460	115	57	68.9	19	0.047	60.5	163.6	100.8	<	327.2	100.8	1.14	Fl-R	Fl-R
FB-3	300	400	354	3.4	34.0	690	41	1.68		3	12.7	380	0.36	0.75	9.5	171	0.28	460	185	93	111.2	29	0.072	92.0	168.9	153.4	<	337.7	153.4	1.21	Fl-R	Fl-R
FB-4	300	400	354	3.4	34.0	690	41	1.68		4	12.7	507	0.48	0.75	9.5	171	0.28	460	210	105	125.9	38	0.092	117.6	173.3	196.0	<	346.6	196.0	1.07	Fl-R	Fl-R
FB-6	300	400	354	3.4	34.0	690	41	1.68		6	12.7	760	0.72	0.75	9.5	171	0.28	460	286	143	171.5	57	0.135	171.9	180.8	286.5	<	361.6	286.5	1.00	Fl-C	Fl-R
FB-8	300	400	335	3.6	34.0	690	41	1.68		8	12.7	1013	1.01	0.75	9.5	171	0.28	460	371	186	222.6	80	0.159	181.4	178.5	302.4	<	357.1	302.4	1.23	Fl-C	Fl-C
HFB-3	300	400	354	3.4	45.0	690	41	1.68		3	12.7	380	0.36	0.99	9.5	171	0.28	460	155	78	93.2	22	0.054	90.5	175.7	150.8	<	351.3	150.8	1.03	Fl-R	Fl-R
HFB-4	300	400	354	3.4	45.0	690	41	1.68		4	12.7	507	0.48	0.99	9.5	171	0.28	460	198	99	119.0	29	0.071	119.3	180.7	198.8	<	361.4	198.8	1.00	Fl-R	Fl-R
HFB-6	300	400	354	3.4	45.0	690	41	1.68		6	12.7	760	0.72	0.99	9.5	171	0.28	460	334	167	200.5	43	0.104	175.9	189.1	293.2	<	378.3	293.2	1.14	Fl-R	Fl-R
HFB-8	300	400	335	3.6	45.0	690	41	1.68		8	12.7	1013	1.01	0.99	9.5	171	0.28	460	363	182	218.0	61	0.140	212.1	187.4	353.5	<	374.8	353.5	1.03	Fl-C	Fl-C
HFB-10	300	400	335	3.6	45.0	690	41	1.68		10	12.7	1267	1.26	0.99	9.5	171	0.28	460	366	183	219.4	76	0.153	231.8	193.4	386.3	<	386.8	386.3	0.95	Fl-C	Fl-C
Barris *et al.* (2009)																																
C-212-D1a	140	190	163	3.7	59.8	1353	63	2.14	G	2	12	226	0.99	0.54	8	70	1.03	335	127	64	38.2	85	0.149	33.3	104.9	111.0	<	209.8	111.0	1.15	Fl-C	Fl-C
C-212-D1b	140	190	163	3.7	59.8	1353	63	2.14		2	12	226	0.99	0.54	8	70	1.03	335	118	59	35.5	85	0.149	33.3	104.9	111.0	<	209.8	111.0	1.07	Fl-C	Fl-C
C-216-D1a	140	190	162	3.7	56.3	995	64	1.55		2	16	402	1.78	0.92	8	70	1.03	335	150	75	45.1	125	0.194	39.9	126.6	132.9	<	253.2	132.9	1.13	Fl-C	Fl-C
C-216-D1b	140	190	162	3.7	56.3	995	64	1.55		2	16	402	1.78	0.92	8	70	1.03	335	143	72	43.0	125	0.194	39.9	126.6	132.9	<	253.2	132.9	1.08	Fl-C	Fl-C
C-316-D1a	140	190	162	3.7	55.2	995	64	1.55		3	16	603	2.67	0.90	8	70	1.03	335	165	82	49.4	191	0.228	46.0	152.1	153.2	<	304.3	153.2	1.07	Fl-C	Fl-C
C-316-D1b	140	190	162	3.7	55.2	995	64	1.55		3	16	603	2.67	0.90	8	70	1.03	335	170	85	50.9	191	0.228	46.0	152.1	153.2	<	304.3	153.2	1.11	Fl-C	Fl-C
C-212-D2a	160	190	143	4.2	59.6	1353	63	2.14		2	12	226	0.99	0.54	8	70	0.90	335	92	46	27.7	86	0.149	28.9	93.1	96.2	<	186.2	96.2	0.96	Fl-C	Fl-C
C-212-D2b	160	190	143	4.2	59.6	1353	63	2.14		2	12	226	0.99	0.54	8	70	0.90	335	85	43	25.5	86	0.149	28.9	93.1	96.2	<	186.2	96.2	0.88	Fl-C	Fl-C
C-216-D2a	160	190	141	4.3	61.7	995	64	1.55		2	16	402	1.79	1.00	8	70	0.90	335	141	70	42.2	115	0.189	36.9	113.8	122.9	<	227.7	122.9	1.14	Fl-C	Fl-C
C-216-D2b	160	190	141	4.3	61.7	995	64	1.55		2	16	402	1.79	1.00	8	70	0.90	335	135	67	40.5	115	0.189	36.9	113.8	122.9	<	227.7	122.9	1.10	Fl-C	Fl-C
C-316-D2a	160	190	141	4.3	60.1	995	64	1.55		3	16	603	2.68	0.98	8	70	0.90	335	144	72	43.2	177	0.222	42.2	134.4	140.7	<	268.8	140.7	1.02	Fl-C	Fl-C
C-316-D2b	160	190	141	4.3	60.1	995	64	1.55		3	16	603	2.68	0.98	8	70	0.90	335	157	79	47.2	177	0.222	42.2	134.4	140.7	<	268.8	140.7	1.12	Fl-C	Fl-C

Notation of FRP types: A: Aramid, B: Basalt, C: Carbon, E-G: Glass fibres with higher electrical resistivity and G: Glass
Notation of failure modes: Fl-R: Rupture of fibres of bars, Fl-C: Concrete Crushing and Sh: Diagonal shear failure

Table 1d Test data and analytical predictions of the examined beams from the present study and the literature

Beam codified name	Geometrical properties				Material properties					FRP reinforcement					Stirrups				Experimental results				Analytical results (according to the proposed model)										Failure mode	
	b (mm)	h (mm)	d (mm)	a/d	f_c (MPa)	f^*_{fu} (MPa)	E_f (GPa)	ε^*_{fu} (%)	FRP type	No	$\varnothing_f$ (mm)	A_f (mm^2)	$\rho_{f,exp}$ (%)	ρ_{fb} (%)	$\varnothing_s$ (mm)	s (mm)	ρ_{sw} (%)	f_{yw} (MPa)	$P_{tot,exp}$ (kN)	V_{exp} (kN)	M_{exp} (kNm)	r_ρ	μ_f	$M_{f,prop}$ (kNm)	$V_{f,prop}$ (kN)	$P^M_{f,calc}$ (kN)		$P^V_{f,calc}$ (kN)	$P_{tot,calc}$ (kN)	$\frac{P_{tot,exp}}{P_{tot,calc}}$	Obs. Fail.	Pred. Fail.
Lee and Kim (2012)																																
A2D8-27	200	400	360	3.6	25.1	1415	62	2.29		2	8	101	0.14	0.21	10	150	0.34	400	86	43	55.7	30	0.076	49.1	158.3	76.2	<	316.5	76.2	1.13	Fl-R	Fl-R
A4D8-27	200	400	360	3.6	25.1	1415	62	2.29		4	8	201	0.28	0.21	10	150	0.34	400	131	65	84.5	59	0.125	81.3	163.9	126.1	<	327.9	126.1	1.04	Fl-C	Fl-C
A6D8-27	200	413	360	3.6	25.1	1415	62	2.29		6	8	302	0.42	0.21	10	150	0.34	400	176	88	113.4	89	0.149	96.9	168.3	150.3	<	336.5	150.3	1.17	Fl-C	Fl-C
A2D8-45	200	400	360	3.6	45.4	1415	62	2.29	A	2	8	101	0.14	0.37	10	150	0.34	400	74	37	47.6	16	0.042	49.4	165.3	76.6	<	330.7	76.6	0.96	Fl-R	Fl-R
A3D8-45	200	400	360	3.6	45.4	1415	62	2.29		3	8	151	0.21	0.37	10	150	0.34	400	126	63	81.4	25	0.063	74.1	169.2	114.9	<	338.4	114.9	1.10	Fl-R	Fl-R
A3D10-45	200	400	360	3.6	45.4	1415	62	2.29		3	10	236	0.33	0.37	10	150	0.34	400	171	85	110.1	38	0.096	113.0	174.8	175.1	<	349.5	175.1	0.97	Fl-C	Fl-R
A4D10-45	200	400	360	3.6	45.4	1415	62	2.29		4	10	314	0.44	0.37	10	150	0.34	400	216	108	139.6	51	0.117	137.7	178.9	213.5	<	357.8	213.5	1.01	Fl-C	Fl-C
C2D8-27	200	400	360	3.6	25.1	2542	143	1.78		2	8	101	0.14	0.14	10	150	0.34	400	153	77	98.9	55	0.130	84.6	164.3	131.1	<	328.6	131.1	1.17	Fl-C	Fl-C
C4D8-27	200	400	360	3.6	25.1	2542	143	1.78		4	8	201	0.28	0.14	10	150	0.34	400	201	101	129.8	110	0.177	115.2	172.4	178.5	<	344.9	178.5	1.13	Fl-C	Fl-C
C4D10-27	200	400	360	3.6	25.1	2542	143	1.78	C	4	10	314	0.44	0.14	10	150	0.34	400	243	121	156.7	172	0.211	137.3	180.5	212.8	<	361.0	212.8	1.14	Fl-C	Fl-C
C5D10-27	200	413	360	3.6	25.1	2542	143	1.78		5	10	393	0.55	0.14	10	150	0.34	400	211	106	136.1	215	0.228	148.3	184.8	230.0	<	369.7	230.0	0.92	Fl-C	Fl-C
Kim and Jang (2013)																																
C-2.5-R1-1	200	250	216	2.5	30	2130	146	1.46		2	9	127	0.30	0.24	-	-	-	-	69	34	18.5	84	0.171	47.6	28.2	176.9	>	56.4	56.4	1.22	Sh	Sh
C-2.5-R2-1	150	250	216	2.5	30	2130	146	1.46		2	9	127	0.39	0.24	-	-	-	-	54	27	14.5	112	0.190	39.7	23.0	147.4	>	46.1	46.1	1.17	Sh	Sh
C-2.5-R2-2	150	250	216	2.5	30	2130	146	1.46		2	9	127	0.39	0.24	-	-	-	-	43	22	11.6	112	0.190	39.7	23.0	147.4	>	46.1	46.1	0.94	Sh	Sh
C-2.5-R3-1	150	250	214	2.5	30	2023	148	1.37		2	13	265	0.83	0.27	-	-	-	-	53	26	14.1	227	0.250	51.3	28.9	192.2	>	57.8	57.8	0.92	Sh	Sh
C-2.5-R3-2	150	250	214	2.5	30	2023	148	1.37		2	13	265	0.83	0.27	-	-	-	-	48	24	12.9	227	0.250	51.3	28.9	192.2	>	57.8	57.8	0.84	Sh	Sh
C-3.5-R1-1	200	250	216	3.5	30	2130	146	1.46		2	9	127	0.30	0.24	-	-	-	-	50	25	18.7	84	0.171	47.6	27.2	126.3	>	54.5	54.5	0.91	Sh	Sh
C-3.5-R1-2	200	250	216	3.5	30	2130	146	1.46		2	9	127	0.30	0.24	-	-	-	-	65	32	24.3	84	0.171	47.6	27.2	126.3	>	54.5	54.5	1.18	Sh	Sh
C-3.5-R2-1	150	250	216	3.5	30	2130	146	1.46	C	2	9	127	0.39	0.24	-	-	-	-	45	23	17.0	112	0.190	39.7	23.4	105.3	>	46.7	46.7	0.97	Sh	Sh
C-3.5-R2-2	150	250	216	3.5	30	2130	146	1.46		2	9	127	0.39	0.24	-	-	-	-	60	30	22.5	112	0.190	39.7	23.4	105.3	>	46.7	46.7	1.28	Sh	Sh
C-3.5-R3-1	150	250	214	3.5	30	2023	148	1.37		2	13	265	0.83	0.27	-	-	-	-	62	31	23.2	227	0.250	51.3	27.9	137.3	>	55.7	55.7	1.12	Sh	Sh
C-3.5-R3-2	150	250	214	3.5	30	2023	148	1.37		2	13	265	0.83	0.27	-	-	-	-	54	27	20.0	227	0.250	51.3	27.9	137.3	>	55.7	55.7	0.96	Sh	Sh
C-4.5-R1-1	200	250	216	4.5	30	2130	146	1.46		2	9	127	0.30	0.24	-	-	-	-	51	26	24.7	84	0.171	47.6	26.3	98.3	>	52.5	52.5	0.97	Sh	Sh
C-4.5-R1-2	200	250	216	4.5	30	2130	146	1.46		2	9	127	0.30	0.24	-	-	-	-	52	26	25.3	84	0.171	47.6	26.3	98.3	>	52.5	52.5	0.99	Sh	Sh
C-4.5-R2-1	150	250	216	4.5	30	2130	146	1.46		2	9	127	0.39	0.24	-	-	-	-	51	25	24.6	112	0.190	39.7	21.4	81.9	>	42.9	42.9	1.18	Sh	Sh

Notation of FRP types: A: Aramid, B: Basalt, C: Carbon, E-G: Glass fibres with higher electrical resistivity and G: Glass
Notation of failure modes: Fl-R: Rupture of fibres of bars, Fl-C: Concrete Crushing and Sh: Diagonal shear failure

Table 1e Test data and analytical predictions of the examined beams from the present study and the literature

Beam codified name	Geometrical properties				Material properties					FRP reinforcement					Stirrups				Experimental results				Analytical results (according to the proposed model)									Failure mode	
	b (mm)	h (mm)	d (mm)	a/d	f_c (MPa)	f^*_{fu} (MPa)	E_f (GPa)	ε^*_{fu} (%)	FRP type	No	$\varnothing_f$ (mm)	A_f (mm^2)	$\rho_{f,exp}$ (%)	ρ_{fb} (%)	$\varnothing_s$ (mm)	s (mm)	ρ_{sw} (%)	f_{yw} (MPa)	$P_{tot,exp}$ (kN)	V_{exp} (kN)	M_{exp} (kNm)	r_ρ	μ_f	$M_{f,prop}$ (kNm)	$V_{f,prop}$ (kN)	$P^M_{f,calc}$ (kN)		$P^V_{f,calc}$ (kN)	$P_{tot,calc}$ (kN)	$\frac{P_{tot,exp}}{P_{tot,calc}}$	Obs. Fail.	Pred. Fail.
Kim and Jang (2013) *(continued)*																																
C-4.5-R2-2	150	250	216	4.5	30	2130	146	1.46		2	9	127	0.39	0.24	-	-	-	-	45	23	21.9	112	0.190	39.7	21.4	81.9	>	42.9	42.9	1.05	Sh	Sh
C-4.5-R3-1	150	250	214	4.5	30	2023	148	1.37	C	2	13	265	0.83	0.27	-	-	-	-	54	27	26.0	227	0.250	51.3	26.8	106.8	>	53.7	53.7	1.01	Sh	Sh
C-4.5-R3-2	150	250	214	4.5	30	2023	148	1.37		2	13	265	0.83	0.27	-	-	-	-	56	28	26.9	227	0.250	51.3	26.8	106.8	>	53.7	53.7	1.04	Sh	Sh
G-2.5-R1-1	200	250	216	2.5	30	980	48	2.03		2	9	127	0.30	0.39	-	-	-	-	49	25	13.3	37	0.091	25.4	21.0	94.1	>	41.9	41.9	1.18	Sh	Sh
G-2.5-R2-1	150	250	216	2.5	30	980	48	2.03		2	9	127	0.39	0.39	-	-	-	-	48	24	12.9	49	0.120	25.1	17.1	93.1	>	39.1	39.1	1.23	Sh	Sh
G-2.5-R2-2	150	250	216	2.5	30	980	48	2.03		2	9	127	0.39	0.39	-	-	-	-	47	23	12.5	49	0.120	25.1	17.1	93.1	>	39.1	39.1	1.19	Sh	Sh
G-2.5-R3-1	150	250	214	2.5	30	941	49	1.92		2	13	265	0.83	0.43	-	-	-	-	51	25	13.5	100	0.165	33.8	21.3	126.8	>	44.7	44.7	1.13	Sh	Sh
G-2.5-R3-2	150	250	214	2.5	30	941	49	1.92		2	13	265	0.83	0.43	-	-	-	-	55	28	14.7	100	0.165	33.8	21.3	126.8	>	44.7	44.7	1.23	Sh	Sh
G-3.5-R1-1	200	250	216	3.5	30	980	48	2.03		2	9	127	0.30	0.39	-	-	-	-	50	25	18.7	37	0.091	25.4	23.1	67.2	>	46.3	46.3	1.07	Sh	Sh
G-3.5-R1-2	200	250	216	3.5	30	980	48	2.03		2	9	127	0.30	0.39	-	-	-	-	55	28	20.9	37	0.091	25.4	23.1	67.2	>	46.3	46.3	1.20	Sh	Sh
G-3.5-R2-1	150	250	216	3.5	30	980	48	2.03		2	9	127	0.39	0.39	-	-	-	-	40	20	15.0	49	0.120	25.1	16.5	66.5	>	37.7	37.7	1.05	Sh	Sh
G-3.5-R2-2	150	250	216	3.5	30	980	48	2.03	G	2	9	127	0.39	0.39	-	-	-	-	42	21	15.8	49	0.120	25.1	16.5	66.5	>	37.7	37.7	1.11	Sh	Sh
G-3.5-R3-1	150	250	214	3.5	30	941	49	1.92		2	13	265	0.83	0.43	-	-	-	-	35	18	13.2	100	0.165	33.8	20.6	90.6	>	41.2	41.2	0.86	Sh	Sh
G-3.5-R3-2	150	250	214	3.5	30	941	49	1.92		2	13	265	0.83	0.43	-	-	-	-	40	20	14.8	100	0.165	33.8	20.6	90.6	>	41.2	41.2	0.96	Sh	Sh
G-4.5-R1-1	200	250	216	4.5	30	980	48	2.03		2	9	127	0.30	0.39	-	-	-	-	36	18	17.6	37	0.091	25.4	19.6	52.3	>	39.2	39.2	0.93	Sh	Sh
G-4.5-R1-2	200	250	216	4.5	30	980	48	2.03		2	9	127	0.30	0.39	-	-	-	-	41	20	19.6	37	0.091	25.4	19.6	52.3	>	39.2	39.2	1.03	Sh	Sh
G-4.5-R2-1	150	250	216	4.5	30	980	48	2.03		2	9	127	0.39	0.39	-	-	-	-	35	17	16.8	49	0.120	25.1	15.9	51.7	>	31.8	31.8	1.09	Sh	Sh
G-4.5-R2-2	150	250	216	4.5	30	980	48	2.03		2	9	127	0.39	0.39	-	-	-	-	32	16	15.4	49	0.120	25.1	15.9	51.7	>	31.8	31.8	1.00	Sh	Sh
G-4.5-R3-1	150	250	214	4.5	30	941	49	1.92		2	13	265	0.83	0.43	-	-	-	-	38	19	18.4	100	0.165	33.8	19.9	70.5	>	39.7	39.7	0.96	Sh	Sh
G-4.5-R3-2	150	250	214	4.5	30	941	49	1.92		2	13	265	0.83	0.43	-	-	-	-	42	21	19.9	100	0.165	33.8	19.9	70.5	>	39.7	39.7	1.05	Sh	Sh
Refai *et al.* (2015)																																
2G12	230	300	259	4.8	40.0	1000	50	2.00		2	12	226	0.38	0.52	8	100	0.44	520	78	39	49.0	36	0.090	55.5	156.6	88.7	<	313.3	88.7	0.88	Fl-R	Fl-R
3G12	230	300	230	5.4	40.0	1000	50	2.00	G	3	12	339	0.64	0.52	8	100	0.44	520	86	43	53.8	61	0.133	65.0	146.4	104.0	<	292.8	104.0	0.83	Fl-C	Fl-C
3G16	230	300	234	5.3	40.0	1000	50	2.00		3	16	603	1.12	0.52	8	100	0.44	520	111	56	69.6	107	0.168	84.7	164.7	135.6	<	329.4	135.6	0.82	Fl-C	Fl-C

Notation of FRP types: A: Aramid, B: Basalt, C: Carbon, E-G: Glass fibres with higher electrical resistivity and G: Glass
Notation of failure modes: Fl-R: Rupture of fibres of bars, Fl-C: Concrete Crushing and Sh: Diagonal shear failure

Table 1f Test data and analytical predictions of the examined beams from the present study and the literature

Beam codified name	Geometrical properties				Material properties					FRP reinforcement					Stirrups				Experimental results				Analytical results (according to the proposed model)											Failure mode	
	b (mm)	h (mm)	d (mm)	a/d	f_c (MPa)	f^*_{fu} (MPa)	E_f (GPa)	ε^*_{fu} (%)	FRP type	No	$\varnothing_f$ (mm)	A_f (mm^2)	$\rho_{f,exp}$ (%)	ρ_{fb} (%)	$\varnothing_s$ (mm)	s (mm)	ρ_{sw} (%)	f_{yw} (MPa)	$P_{tot,exp}$ (kN)	V_{exp} (kN)	M_{exp} (kNm)	r_ρ	μ_f	$M_{f,prop}$ (kNm)	$V_{f,prop}$ (kN)	$P^M_{f,calc}$ (kN)		$P^V_{f,calc}$ (kN)	$P_{tot,calc}$ (kN)	$\frac{P_{tot,exp}}{P_{tot,calc}}$	Obs. Fail.	Pred. Fail.
Zhang *et al.* (2015)																																		
B1	180	230	209	2.9	23.6	1075	46	2.32	B	2	6	57	0.15	0.25	8	100	0.56	335	54	27	16.3	26	0.068	12.6	77.5	42.1	<	154.9	42.1	1.29	Fl-R	Fl-R
B2	180	230	209	2.9	28.0	1075	46	2.32		3	6	85	0.23	0.30	8	100	0.56	335	77	38	23.0	33	0.086	18.9	80.2	63.1	<	160.4	63.1	1.21	Fl-R	Fl-R
B3	180	230	208	2.9	33.9	1075	46	2.32		3	8	129	0.34	0.36	8	100	0.56	335	92	46	27.7	41	0.103	27.2	83.8	90.6	<	167.5	90.6	1.02	Fl-R	Fl-R
B4	180	230	208	2.9	27.0	1204	49	2.46		3	8	151	0.40	0.24	8	100	0.56	335	96	48	28.9	67	0.128	26.9	83.1	89.7	<	166.2	89.7	1.07	Fl-C	Fl-C
B5	180	230	207	2.9	30.0	1100	44	2.48		3	10	207	0.56	0.29	8	100	0.56	335	118	59	35.5	76	0.134	31.0	85.7	103.4	<	171.4	103.4	1.14	Fl-C	Fl-C
B6	180	230	207	2.9	34.0	1100	44	2.48		3	10	236	0.63	0.33	8	100	0.56	335	117	59	35.1	76	0.134	35.1	88.0	117.1	<	176.1	117.1	1.00	Fl-C	Fl-C
Ovitigala *et al.* (2016)																																		
3-10L	200	300	261	4.4	35.9	1121	55	2.03	B	3	10	236	0.45	0.41	9.5	75	0.95	460	102	51	58.8	54	0.125	60.9	240.1	105.9	<	480.2	105.9	0.96	Fl-C	Fl-C
2-13L	200	300	259	4.4	35.9	1082	53	2.06		2	13	265	0.51	0.42	9.5	75	0.95	460	100	50	57.7	59	0.130	62.6	244.2	108.9	<	488.5	108.9	0.92	Fl-C	Fl-C
4-10L	200	300	261	4.4	35.9	1121	55	2.03		4	10	314	0.60	0.41	9.5	75	0.95	460	110	55	63.0	72	0.140	68.2	245.1	118.6	<	490.1	118.6	0.92	Fl-C	Fl-C
3-13M	200	300	259	4.4	35.9	1082	53	2.06		3	13	398	0.77	0.42	9.5	75	0.95	460	116	58	66.9	88	0.152	73.2	254.2	127.3	<	508.4	127.3	0.91	Fl-C	Fl-C
2-16M	200	300	258	4.5	35.9	1117	52	2.15		2	16	402	0.78	0.39	9.5	75	0.95	460	122	61	70.1	92	0.154	73.3	261.2	127.5	<	522.3	127.5	0.96	Fl-C	Fl-C
3-16M	200	300	258	4.5	35.9	1117	52	2.15		3	16	603	1.17	0.39	9.5	75	0.95	460	153	77	88.2	138	0.181	86.2	279.5	149.9	<	559.0	149.9	1.02	Fl-C	Fl-C
2-25H	200	300	253	4.5	35.9	1089	53	2.05		2	25	982	1.94	0.42	9.5	75	0.95	460	165	82	94.8	225	0.221	101.3	405.9	176.2	<	811.8	176.2	0.93	Fl-C	Fl-C
3-25H	200	300	253	4.5	35.9	1089	53	2.05		3	25	1473	2.91	0.42	9.5	75	0.95	460	193	96	110.7	337	0.254	116.7	507.2	203.0	<	1015	203.0	0.95	Fl-C	Fl-C
Elgabbas *et al.* (2017)																																		
B-3#8	200	300	258	4.3	40.0	1655	65	2.56	B	3	8	151	0.29	0.25	10	100	0.79	450	96	48	52.9	45	0.106	56.4	207.2	102.6	<	414.4	102.6	0.94	Fl-C	Fl-C
B-5#8	200	300	244	4.5	40.0	1655	65	2.56		5	8	251	0.52	0.25	10	100	0.79	450	119	60	65.5	79	0.136	64.8	215.2	117.8	<	430.4	117.8	1.01	Fl-C	Fl-C
B-2#12	200	300	256	4.3	40.0	1760	69	2.54		2	12	226	0.44	0.24	10	100	0.79	450	99	49	54.4	72	0.130	68.2	212.9	123.9	<	425.8	123.9	0.80	Fl-C	Fl-C
B-3#12	200	300	256	4.3	40.0	1760	69	2.54		3	12	339	0.66	0.24	10	100	0.79	450	122	61	67.0	109	0.153	80.2	221.9	145.8	<	443.2	145.8	0.84	Fl-C	Fl-C
B-2#16	200	300	254	4.3	40.0	1724	65	2.66		2	16	402	0.79	0.24	10	100	0.79	450	129	65	71.1	127	0.161	83.1	226.3	151.1	<	452.5	151.1	0.86	Fl-C	Fl-C
B-3#16	200	300	254	4.3	40.0	1724	65	2.66		3	16	603	1.19	0.24	10	100	0.79	450	166	83	91.0	190	0.191	98.6	240.7	179.2	<	481.3	179.2	0.92	Fl-C	Fl-C

Notation of FRP types: A: Aramid, B: Basalt, C: Carbon, E-G: Glass fibres with higher electrical resistivity and G: Glass
Notation of failure modes: Fl-R: Rupture of fibres of bars, Fl-C: Concrete Crushing and Sh: Diagonal shear failure

$$\rho_f = \frac{A_f}{bd} = \frac{157}{200\times 200} = 0.39\%$$

$$\rho_{sw} = \frac{A_{sw}}{bs} = \frac{57}{200\times 200} = 0.14\%$$

- Size effect coefficient, ζ:

$$\zeta = 1.2 - 0.2\text{a} = 1.2 - 0.2\times 1 = 1.0 > 0.65$$

- Modular ratio, a_e:

$$\alpha_e = \frac{E_f}{E_c} = \frac{130}{30} = 4.29$$

- Neutral axis depth, c:

$$\xi = \alpha_e\rho_f\left(-1+\sqrt{1+\frac{2}{\alpha_e\rho_f}}\right)\rightarrow$$

$$\xi = 4.29\times 0.39\%\left(-1+\sqrt{1+\frac{2}{4.29\times 0.39\%}}\right) = 0.167$$

$$c = \xi d = 0.167\times 200 = 33\text{ mm}$$

- Inclination angle of the critical shear crack, θ, and average crack spacing of the inclined cracks, $s_{m\theta}$:

$$\theta = \tan^{-1}\left(\frac{d-c}{0.85d}\right) = \tan^{-1}\left(\frac{200-33}{0.85\times 200}\right) = 44.4^\circ$$

$$s_{m\theta} = \frac{d-c}{2}\cos\theta = \frac{200-33}{2}\cos(44.4^\circ) = 59\text{ mm}$$

- Ultimate tensile strain of concrete, $\varepsilon_{ct,u}$, and vertical projection, c_w:

$$\varepsilon_{ct,u} = \frac{f_{ct}}{E_c}\left(1+\frac{2G_fE_c}{f_{ct}^2 s_{m\theta}}\right)\rightarrow$$

$$\varepsilon_{ct,u} = \frac{2.42}{30,000}\left(1+\frac{2\times 0.125\times 30,000}{2.42^2\times 59}\right) = 0.183\%$$

$$c_w = (d-c)\frac{\varepsilon_{ct,u}}{\varepsilon_r}\sin^2\theta\rightarrow$$

$$c_w = (200-33)\frac{0.00183}{0.01}\times\sin^2(44.4^\circ) = 14.8\text{ mm}$$

- Coefficient β_w:

$$\beta_w = \frac{0.85-0.5\frac{c_w}{d}\cot\theta}{\cos^2\theta}\rightarrow$$

$$\beta_w = \frac{0.85-0.5\frac{14.8}{200}\cot(44.4^\circ)}{\cos^2(44.4^\circ)} = 1.592$$

- Shear force resisted along the critical crack, V_w:

$$V_w = 42.5\frac{f_{ct}^2}{E_c}\sin^2\theta\left(1+\frac{2G_fE_c}{f_{ct}^2 s_{m\theta}}\right)bd =$$

$$= 42.5\frac{2.42^2}{30,000}\times\sin^2(44.4^\circ)\times$$

$$\times\left(1+\frac{2\times 0.125\times 30,000}{2.42^2\times 59}\right)\times 200\times 200\times 10^{-3}\rightarrow$$

$$V_w = 3.6\text{ kN}$$

- Contribution of the transverse reinforcement (steel stirrups) to the shear strength, V_s:

$$V_s = 0.85\rho_{sw}f_{yw}bd\rightarrow$$

$$V_s = 0.85\times 0.0014\times 310\times 200\times 200\times 10^{-3} = 14.8\text{ kN}$$

- Non-dimensional moment μ^*:

$$\mu^* = \mu + \beta_w\frac{V_w}{f_{ct}bd} + \beta_s\frac{V_s}{f_{ct}bd} = 0.2 +$$

$$+1.586\frac{3.7\times 10^3}{2.42\times 200\times 200} + 0.425\frac{14.8\times 10^3}{2.42\times 200\times 200}\rightarrow$$

$$\mu^* = 0.325$$

- Contribution of the un-cracked concrete chord to the shear strength, V_c:

$$V_c = \zeta(1.072-0.01\alpha_e)\times$$

$$\times\left[(0.903+0.26\mu^*)\xi + 0.012 + 0.1325\mu^*\right]f_{ct}bd =$$

$$= 1.0(1.072-0.01\times 4.29)\times$$

$$\times\left[(0.903+0.26\times 0.325)0.167 +\right.$$

$$\left.+0.012+0.1325\times 0.325\right]\times 2.42\times 200^2\times 10^{-3}\rightarrow$$

$$V_c = 22.0\text{ kN}$$

- Contribution of the longitudinal FRP bars to the shear strength, V_ℓ:

$$V_\ell = 0.0064E_fA_f\frac{\varnothing_f^2 d}{s^3}\frac{1}{1-\xi} =$$

$$= 0.0064\times 130,000\times 157\frac{10^2\times 200}{200^3}\frac{1}{1-0.167}\rightarrow$$

$$V_\ell = 0.4\text{ kN}$$

Note: The calculated value of V_ℓ is very low and confirms the consideration of Oller *et al.* (2015) that the contribution of the longitudinal FRP bars as dowel action to the shear strength is insignificant and, therefore, it can be neglected.

- Ultimate shear strength, V_f:

$$V_f = V_c + V_w + V_s + V_\ell = 22.0 + 3.6 + 14.8 + 0.4\rightarrow$$

$$V_f = 40.8\text{ kN}$$

- Total strength in terms of applied load, $P_{f,calc}^V$, which corresponds to the shear strength, V_f:

$$P_{f,calc}^V = 2V_f = 2\times 40.8 = 81.6\text{ kN}$$

4.3 Ultimate strength and predicted failure mode

- According to the proposed methodology the ultimate strength of the beam "F10" is:

$$P_{tot,calc} = \min\left(P_{f,calc}^M, P_{f,calc}^V\right) = \min(86.1, 81.6) = 81.6\text{ kN}$$

The experimental ultimate strength of the beam "F10" is $P_{tot,exp}$=83.0 kN (see Table 1a), which is very close to the calculated one. Further, typical shear failure due to concrete diagonal tensional failure occurred, as it is correctly predicted by the proposed analysis.

5. Conclusions

The flexural/shear capacity and the expected failure mode of concrete beams with longitudinal FRP bars, with or without transverse shear reinforcement are evaluated using a feasible and easy-to-apply analytical approach. Specially developed general charts that adopt the design provisions of

ACI 440.1R-15 are used for the calculation of the flexural strength. These charts include non-dimensional variables in order to provide hand calculations and to be applied in sections with various geometrical properties, concrete grade and FRP properties. A shear model that combines three established theoretical considerations is also proposed. A unified flexural/shear computational approach that enables software implementation is developed and experimentally verified. Two slender RC beams with carbon FRP bars and low ratio of transverse shear reinforcement have been tested in four-point bending load. The under-reinforced beam against flexure failed due to FRP rupture in the tensional zone, whereas the over-reinforced one exhibited brittle shear failure due to concrete diagonal tension. Further, the validity of the proposed analytical method is thoroughly verified by comparisons between analytical predictions and test data of 138 concrete beams with various types of FRP bars, which failed under different modes compiled from the present study and 13 existing experimental works of the literature. From these comparisons it is observed that the developed approach predicts with satisfactory accuracy the ultimate load-bearing capacity and the expected failure mode for the majority of the examined cases.

References

Abdul-Salam, B., Farghaly, A.S. and Benmokrane, B. (2016), "Mechanisms of shear resistance of one-way concrete slabs reinforced with FRP bars", *Constr. Build. Mater.*, **127**, 959-970.

ACI Committee 440 (2015), Guide for the Design and Construction of Structural Concrete Reinforced with FRP bars, ACI 440.1R-15, American Concrete Institute, Farmington Hills, Detroit, Michigan, USA.

Alam, M.S., Youssef, M.A. and Nehdi, M.L. (2010), "Exploratory investigation on mechanical anchors for connecting SMA bars to steel or FRP bars", *Mater. Struct.*, **43**(1), 91-107.

Ashour, A.F. (2006), "Flexural and shear capacities of concrete beams reinforced with GFRP bars", *Constr. Build. Mater.*, **20**(10), 1005-1015.

Barris, L., Torres, Ll., Turon, A., Baena, M. and Catalan, A. (2009), "An experimental study of the flexural behaviour of GFRP RC beams and comparison with prediction models", *Compos. Struct.*, **91**(3), 286-295.

Bencardino, F., Condello, A. and Ombres, L. (2016), "Numerical and analytical modeling of concrete beams with steel, FRP and hybrid FRP-steel reinforcements", *Compos. Struct.*, **140**, 53-65.

Bouguerra, K., Ahmed, E.A., El-Gamal, S. and Benmokrane, B. (2011), "Testing of full-scale concrete bridge deck slabs reinforced with fiber-reinforced polymer (FRP) bars", *Constr. Build. Mater.*, **25**, 3956-3965.

Bousias, S.N., Triantafillou, T.C., Fardis, M.N., Spathis, L. and O' Regan, B.A. (2004), "Fiber-reinforced polymer retrofitting of rectangular reinforced concrete columns with or without corrosion", *ACI Struct. J.*, **101**(4), 512-520.

Bui, L.V.H., Stitmannaithum, B. and Ueda, T. (2017), "Mechanical performances of concrete beams with hybrid usage of steel and FRP tension reinforcement", *Comput. Concrete*, **20**(4), 391-407.

Canadian Standards Association (2012), Design and Construction of Building Components with Fibre-Reinforced Polymers, CSA S806-12, Rexdale, Toronto, Canada.

Chalioris, C.E., Kosmidou, P.-M.K., Panagiotopoulos, T.A. and Karayannis, C.G. (2016), "Flexural and cracking behaviour of concrete beans reinforced with FRP bars", *Proceedings of the 6th International Conference on Concrete Repair-Concrete Solutions*, Thessaloniki, Greece, June.

CNR-DT 203 (2007), Guide for the Design and Construction of Concrete Structures Reinforced with Fiber-Reinforced Polymer Bars, CNR-DT 203/2006, National Research Council, Rome, Italy.

El-Helou, R.G. and Aboutaha, R.S. (2015), "Analysis of rectangular hybrid steel-GFRP reinforced concrete beam columns", *Comput. Concrete*, **16**(2), 245-260.

El-Sayed, A.K. and Soudki, K. (2011), "Evaluation of shear design equations of concrete beams with FRP reinforcement", *J. Compos. Constr.*, **15**(1), 9-20.

El-Sayed, A.K., El-Salakawy, E.F. and Benmokrane, B. (2006), "Shear strength of FRP-reinforced concrete beams without transverse reinforcement", *ACI Struct. J.*, **103**(2), 235-242.

Elgabbas, F., Ahmed, E.A. and Benmokrane, B. (2017), "Flexural behavior of concrete beams reinforced with ribbed basalt-FRP bars under static loads", *J. Compos. Constr.*, **21**(3), 04016098.

European Committee for Standardization (2004), EN 1992-1-1 Eurocode 2: Design of Concrete Structures-Part 1-1: General Rules and Rules for Buildings, CEN, Brussels, Belgium.

Fang, H., Xu, X., Liu, W., Qi, Y., Bai, Y., Zhang, B. and Hui, D. (2016), "Flexural behavior of composite concrete slabs reinforced by FRP grid facesheets", *Compos. Part B: Eng.*, **92**, 46-62.

Fib bulletin 40 (2007), FRP Reinforcement in RC Structures, International Federation for Structural Concrete, Lausanne.

Ghatefar, A., ElSalakawy, E. and Bassuoni, M.T. (2017), "A model for the restrained shrinkage behavior of concrete bridge deck slabs reinforced with FRP bars", *Comput. Concrete*, **20**(2), 215-227.

Goldston, M.W., Remennikov, A. and Sheikh, M.N. (2016), "Experimental investigation of the behaviour of concrete beams reinforced with GFRP bars under static and impact loading", *Eng. Struct.*, **113**, 220-232.

Goldston, M.W., Remennikov, A. and Sheikh, M.N. (2017), "Flexural behaviour of GFRP reinforced high strength and ultra high strength concrete beams", *Constr. Build. Mater.*, **131**, 606-617.

Ha, G.J., Cho, C.G., Kang, H.W. and Feo, L. (2013), "Seismic improvement of RC beam-column joints using hexagonal CFRP bars combined with CFRP sheets", *Compos. Struct.*, **95**, 464-470.

Johnson, D.T. and Sheikh, S.A. (2016), "Experimental investigation of glass fiber-reinforced polymer-reinforced normal-strength concrete beams", *ACI Struct. J.*, **113**(6), 1165-1174.

Ju, M., Park C. and Kim, Y. (2017), "Flexural behavior and a modified prediction of deflection of concrete beam reinforced with a ribbed GFRP bars", *Comput. Concrete*, **19**(6), 631-639.

Kang, T.H.K. and Ary, M.I. (2012), "Shear-strengthening of reinforced & prestressed concrete beams using FRP: Part II - Experimental investigation", *Int. J. Concrete Struct. Mater.*, **6**(1), 49-57.

Kim, C.H. and Jang, H.S. (2014), "Concrete shear strength of normal and lightweight concrete beams reinforced with FRP bars", *J. Compos. Constr.*, **18**(2), 2-10.

Konsta-Gdoutos, M. and Karayannis, C. (1998), "Flexural behaviour of concrete beams reinforced with FRP bars", *Adv. Composite Let.*, **7**(5), 133-137.

Lau, D. and Pam, H.J. (2010), "Experimental study of hybrid FRP reinforced concrete beams", *Eng. Struct.*, **32**(12), 3857-3865.

Lee, Y.H. and Kim, M.S. (2012), "Flexural behavior and deflection prediction of concrete beams reinforced with AFRP and CFRP bars", *ACI Struct. J.*, **284**, 1-26.

Liang, J.F., Deng, Y., Hu, M. and Tang, D. (2017b), "Cyclic performance of concrete beams reinforced with CFRP

prestressed prisms", *Comput. Concrete*, **19**(3), 227-232.
Liang, J.F., Yu, D. and Yu, B. (2016), "Flexural behavior of concrete beams reinforced with CFRP prestressed prisms", *Comput. Concrete*, **17**(3), 295-304.
Liang, J.F., Yu, D., Xie, S. and Li, J. (2017a), "Flexural behaviour of reinforced concrete beams strengthened with NSM CFRP prestressed prisms", *Struct. Eng. Mech.*, **62**(3), 291-295.
Marí, A., Bairán, J., Cladera, A., Oller, E. and Ribas, C. (2015), "Shear-flexural strength mechanical model for the design and assessment of reinforced concrete beams", *Struct. Infrastr. Eng.*, **11**(11), 1399-1419.
Marí, A., Cladera, A., Oller, E. and Bairán, J. (2014), "Shear design of FRP reinforced concrete beams without transverse reinforcement", *Compos. Part B: Eng.*, **57**(2), 228-241.
Masmoudi, R., Thériault, M. and Benmokrane, B. (1998), "Flexural behavior of concrete beams reinforced with deformed fiber reinforced plastic reinforcing rods", *ACI Struct. J.*, **95**(6), 665-675.
Oller, E., Marí, A., Bairán, J. and Cladera, A. (2015), "Shear design of reinforced concrete beams with FRP longitudinal and transverse reinforcement", *Compos. Part B: Eng.*, **74**(1), 104-122.
Ovitigala, T., Ibrahim, M.A. and Issa, M.A. (2016), "Serviceability and ultimate load behavior of concrete beams reinforced with basalt fiber-reinforced polymer bars", *ACI Struct. J.*, **113**(4), 757-768.
Qin, R., Zhou, A. and Lau, D. (2017), "Effect of reinforcement ratio on the flexural performance of hybrid FRP reinforced concrete beams", *Compos. Part B: Eng.*, **108**, 200-209.
Rafi, M.M., Nadjai, A., Ali, F. and Talamona, D. (2008), "Aspects of behaviour of CFRP reinforced concrete beams in bending", *Constr. Build. Mater.*, **22**(3), 277-285.
Refai, A.E., Aded, F. and Al-Rahmani, A. (2015), "Structural performance and serviceability of concrete beams reinforced with hybrid (GFRP and steel) bars", *Constr. Build. Mater.*, **96**, 518-559.
Said, M., Adam, M.A., Mahmoud, A.A. and Shanour, A.S. (2016), "Experimental and analytical shear evaluation of concrete beams reinforced with glass fiber reinforced polymers bars", *Constr. Build. Mater.*, **102**, 574-591.
Saikia, B., Kumar, P., Thomas, J., K.S. Nanjunda Rao and Ramaswamy, A. (2007), "Strength and serviceability performance of beams reinforced with GFRP bars in flexure" *Constr. Build. Mater.*, **21**, 1709-1719.
Shin, S., Seo, D. and Han, B. (2009), "Performance of concrete beams reinforced with GFRP bars", *J. Asian Arch. Build. Eng.*, **8**(1), 197-204.
Shraideh, M.S. and Aboutaha, R.S. (2013), "Analysis of steel-GFRP reinforced concrete circular columns", *Comput. Concrete*, **11**(4), 351-364.
Tan, K.H. (2002), "Strength enhancement of rectangular reinforced concrete columns using fiber-reinforced polymer", *J. Compos. Constr.*, **6**(3), 175-183.
Torres, L.l., Neocleous, K. and Pilakoutas, K. (2012), "Design procedure and simplified equations for the flexural capacity of concrete members reinforced with fibre-reinforced polymer bars", *Struct. Concrete*, **13**(2), 119-129.
Toutanji, A.H. and Saafi, M. (2000), "Flexural behavior of concrete beams reinforced with glass fiber-reinforced polymer (GFRP) bars", *ACI Struct. J.*, **97**(5), 712-719.
Tsonos, A.G. (2009), "Ultra-high-performance fiber reinforced concrete: An innovative solution for strengthening old R/C structures and for improving the FRP strengthening method", *WIT Tran. Eng. Sci.*, **64**, 273-284.
Tureyen, A.K. and Frosch, R.J. (2002), "Shear tests of FRP-reinforced concrete beams without stirrups", *ACI Struct. J.*, **99**(4), 427-434.
Vougioukas, E., Zeris, C.A. and Kotsovos, M.D. (2005), "Toward safe and efficient use of fiber-reinforced polymer for repair and strengthening of reinforced concrete structures", *ACI Struct. J.*, **102**(4), 525-534.
Yost, J.R., Gross, S.P. and Dinehart, D.W. (2001), "Shear strength of normal strength concrete beams reinforced with deformed GFRP bars", *J. Compos. Constr.*, **5**(4), 268-275.
Zadeh, H.J. and Nanni, A. (2013), "Reliability analysis of concrete beams internally reinforced with fiber-reinforced polymer bars", *ACI Struct. J.*, **110**(6), 1023-1031.
Zararis, P.D. and Papadakis, G.C. (2001), "Diagonal shear failure and size effect in RC beams without reinforcement", *J. Struct. Eng.*, **127**(7), 733-742.
Zeris, C., Batis, G., Mouloudakis, V. and Marakis J. (2014), "Accelerated corrosion investigation of axially loaded reinforced concrete elements", *Anti-Corros. Meth. Mater.*, **61**(4), 215-223.
Zhang, L., Sun, Y. and Xiong, W. (2015), "Experimental study on the flexural deflections of concrete beam reinforced with Basalt FRP bars", *Mater. Struct.*, **48**(10), 3279-3293.

AW

Notations

a	shear span of the beam, mm.
α_e	modular ratio equal to E_f/E_c.
A_f	area of the tensional longitudinal FRP reinforcement, mm^2.
A_{sw}	area of the steel transverse reinforcement, mm^2.
b, h	width and height (or overall depth) of the cross-section of the beam, mm.
c	neutral axis depth, mm.
C_E	environmental reduction factor for various fiber type and exposure conditions.
d	effective depth of the cross-section of the beam, mm.
$d_{\max}$	maximum aggregate size, mm.
a/d	shear span-to-depth ratio.
E_c	modulus of elasticity of concrete, GPa.
E_f	guaranteed modulus of elasticity of FRP, MPa.
f_c	cylinder compressive strength of concrete, MPa.
f_{ct}	uniaxial tensile strength of concrete, MPa.
$f_{ct,spl}$	splitting tensile strength of concrete, MPa.
f_{fu}	design tensile strength of FRP, considering reductions for service environment, equal to $C_E \times f^*_{fu}$, MPa.
f^*_{fu}	guaranteed ultimate tensile strength of FRP bar, MPa.
f_{yw}	yield tensile strength of the transverse steel reinforcement, MPa.
G_f	fracture of energy of concrete, N/mm.
M_{Ed}	design value of the externally applied bending moment, kNm.
M_{exp}	experimental flexural strength, kNm.
M_f or $M_{f,prop}$	flexural capacity calculated according to the proposed methodology, kNm.
$P^M_{f,calc}$	calculated total strength, which corresponds to the flexural capacity calculated according to the proposed methodology, kN.
$P^V_{f,calc}$	calculated total strength, which corresponds to the shear strength calculated according to the proposed

methodology, kN.

$P_{tot,calc}$ calculated ultimate strength, kN.

$P_{tot,exp}$ ultimate experimental applied load, kN.

$r_{\rho,d}$ non-dimensional design ratio of the FRP reinforcement ratio, ρ_f, to the design balanced ratio, $\rho_{fb,d}$, divided by the design tensile strain of FRP bar, ε_{fu}.

r_{ρ} non-dimensional ratio of the FRP reinforcement ratio, ρ_f, to the balanced ratio, ρ_{fb}, divided by the guaranteed ultimate tensile strain of FRP bar, ε^*_{fu}.

s uniform spacing of the shear reinforcement, mm.

$s_{m\theta}$ average crack spacing of the inclined cracks, mm.

V_c contribution to the shear strength of the un-cracked concrete chord of a beam without shear reinforcement, kN.

V_{exp} experimental shear strength, kN.

V_{ℓ} contribution to the shear strength of the longitudinal reinforcement, kN.

V_f or $V_{f,prop}$ ultimate shear strength calculated according to the proposed methodology, kN.

V_s contribution to the shear strength of the transverse reinforcement, kN.

V_w shear force resisted along the critical crack, kN.

β_1 reduction factor of the concrete compressive strength taken as 0.85 for concrete strength up to 28 MPa; for strength above 28 MPa β_1 is reduced continuously at a rate of 0.05 per each 7 MPa in excess of 28 MPa, but is not taken less than 0.65.

β_s coefficient for the evaluation of the lever arm of the shear force at the transverse stirrups along the critical crack equal to 0.85/2.

β_w coefficient for the evaluation of the lever arm of the residual shear force resisted along the critical crack.

ε_c maximum compressive strain of concrete taken equal to 3‰.

$\varepsilon_{ct,u}$ ultimate tensile strain of concrete.

ε_{fu} design tensile strain of FRP bar equal to $C_E \times \varepsilon^*_{fu}$.

ε^*_{fu} guaranteed ultimate tensile strain of FRP bar equal to f^*_{fu}/E_f.

ε_r strain of the tensional longitudinal FRP reinforcement when shear failure occurs.

θ inclination angle of the critical shear crack, °.

μ_f value of the non-dimensional flexural capacity.

$\mu_{fd,\beta 1}$ value of the non-dimensional design bending moment.

ξ neutral axis depth ratio equal to c/d

ρ_f tensional longitudinal FRP reinforcement ratio equal to A_f/bd, %.

$\rho_{fb,d}$ FRP reinforcement design ratio producing balanced strain conditions, %.

ρ_{fb} FRP reinforcement ratio producing balanced strain conditions for analysis, %.

ρ_{sw} steel transverse reinforcement ratio equal to A_{sw}/bs, %.

$\varnothing_f$ diameter of the tensional longitudinal FRP reinforcement, mm.

$\varnothing_s$ diameter of the steel transverse reinforcement, mm.